A theoretical model of neural maturation in the developing spinal cord

Piyush Joshi[1], and Isaac Skromne[2]*

[1]Division of Pediatric Neuro-oncology, German Cancer Research Center (DKFZ), 69120 Heidelberg, Germany

[2]Current Address: Department of Biology, University of Richmond, 28 Westhampton Way B322, Richmond, Virginia, 23173, United States

***Corresponding author:** (I.S.) Tel.: +1-804-829-8235; Fax: +1-804-289-8871; E-mail: iskromne@richmond.edu

Keywords: CDX, neurogenesis, spinal cord, gene regulatory network, signaling factors

Running title: Mathematical model of spinal cord neural maturation

Abstract

Cellular differentiation is a tightly regulated process under the control of intricate signaling and transcription factors interaction network working in coordination. These interactions make the systems dynamic, robust and stable but also difficult to dissect. In the spinal cord, recent work has shown that a network of FGF, WNT and Retinoic Acid (RA) signaling factors regulate neural maturation by directing the activity of a transcription factor network that contains CDX at its core. Here we have used partial and ordinary (Hill) differential equation based models to understand the spatiotemporal dynamics of the FGF/WNT/RA and the CDX/transcription factor networks, alone and in combination. We show that in both networks, the strength of interaction among network partners impacts the dynamics, behavior and output of the system. In the signaling network, interaction strength determine the position and size of discrete regions of cell differentiation and small changes in the strength of the interactions among networking partners can result in a signal overriding, balancing or oscillating with another signal. We also show that the spatiotemporal information generated by the signaling network can be conveyed to the CDX/transcription network to produces a transition zone that separates regions of high cell potency from regions of cell differentiation, in agreement with most *in vivo* observations. Importantly, both networks have built in robustness to extrinsic disturbances. This analysis provides a model for the interaction conditions underlying spinal cord cell maturation during embryonic axial elongation.

Introduction

Cells sequentially differentiate from high to low potency states, under the guidance of extracellular signals working in coordination with intracellular transcription factors. Signals regulate the individual and network activity of the transcription factors by providing spatial and temporal information [1-4]. In turn, transcriptional network dictates a cell's competence and response to extracellular signals [5-7]. Because signaling information changes the composition of a cell's transcriptional components, this creates an intricate and dynamic cross-regulatory system for guiding cell differentiation that has been challenging to untangle and comprehend [1, 3, 4].

Vertebrate spinal cord provides an advantageous model to study the cross-regulatory dynamics involved in central nervous system development in particular, and differentiation in general. The head (rostral) to tail (caudal) development of spinal cord during vertebrate body extension results into a characteristic spatial separation of temporal differentiation events [8-10], facilitating the study of their regulation. Briefly, the spinal cord neural progenitors (NPs) are derived from a bipotent population of cells located at the caudal most end of the embryo, the neuro-mesodermal progenitors (NMPs). In the early embryo, the region where NMPs reside is known as the caudal lateral epiblast and node streak border, and in the late embryo, the caudal neural hinge [8-10]. During development, NP cells exit the NMP domain rostrally and then, sequentially, transit through different maturation states as they become part of the spinal cord [8, 11, 12].

NP cell maturation is driven by synergistic and antagonistic interactions between the signaling factors FGF, WNT and Retinoic Acid (RA), turning on and off key transcription factors required for caudal-to-rostral maturation events (**Fig 1A**). Current models propose that

65 two opposite signaling gradients regulate spinal cord cell maturation [13]: from caudal/high to
66 rostral/low, FGF and WNT gradients prevents cell differentiation by promoting high potency cell
67 states caudally; whereas an opposite rostral/high to caudal/low gradient of RA secreted from
68 somites promotes cell differentiation rostrally. Importantly, FGF and WNT activity gradient
69 counteract RA activity gradient. In this way, cells located caudally experience high levels of
70 FGF/WNT and no RA, which drives expression of bipotency markers *T/Bra*, *Sox2*, and *Nkx1.2*
71 [11, 14, 15]. T/BRA and SOX2 are transcription factors that repress each other and promote
72 different cell fates, with T/BRA promoting mesoderm and SOX2 promoting neural fates [16-19].
73 In addition, both transcription factors downregulate FGF and WNT, initiating the early
74 differentiation of mesoderm or neural tissues [16]. NMPs that continue to transcribe *Sox2* but not
75 *T/Bra* assume NPs identity and become part of the growing neural plate. As NPs transit through
76 the maturing neural plate, they experience a further gradual loss in FGF and WNT, and a gradual
77 increase in RA signaling. This new environment lead to the caudal-to-rostral downregulation of a
78 third bipotency marker, *Nkx1.2*, and upregulation of the early differentiation gene *Pax6* [20].
79 Subsequently, under RA regulation, PAX6 activates late differentiation genes such as *Ngn2* (**Fig**
80 **1B**) [10, 21, 22]. Recently, we experimentally mapped the interactions of these transcription
81 factors into a gene regulatory network (GRN) and place it in the context of the FGF/WNT-RA
82 signaling network (**Fig 1C**) [12]. This work identified the transcription factor CDX4 as a core
83 system component essential for the sequential maturation of NPs into mature neuronal precursors
84 (**Fig 1C**).

85

86 **Fig 1. Expression domains and network interactions of key signaling and transcription**
87 **factors involved in caudal spinal cord maturation.** (**A**) Schematic representation of the caudal

end of a stage HH10-11 chick embryo (dorsal view). Expression domains of *Fgf8* (red) and *Wnt8c* (magenta) signaling factors, and the Retinoic Acid synthesizing enzyme *Raldh2* (blue), are superimposed on the diagram (based on [23]). Expression domain of relevant transcription factors are indicated on the left (based on [12]). (**B**) Expression domains of key transcription factors involved in caudal spinal cord maturation. Embryos are stage HH10-11. Scale bar is 200μm. Arrowheads indicates the anterior boundary of the last formed somite. Transcription of the *T/Bra* gene along the embryo's midline is in the notochord underlying the neural tissue, where it is absent. (**C**) Postulated gene regulatory network showing interaction between signaling and transcription factors (based on [12, 16, 21, 23]).

Here we use partial and ordinary (Hill) differential equations to dynamically analyze the GRN driving NP cell maturation during early spinal cord development. As the transcription factor network depends upon inputs form the FGF-WNT-RA signaling network, we first analyzed the postulated effectiveness of the signaling network to work as a signaling switch [23]. We then used the resulting signaling dynamics as input to evaluate the performance of the underlying transcription GRN in its ability to generate cell state patterns similar to those observed in experimental models. Our results show that signaling interaction can give rise to various developmentally observed phenotypes based on a limited subset of interaction parameters, and these behaviors are robust and stable to perturbations. These robust behaviors are due to strong cross-regulation interactions between system elements. Our results suggests that the dominant predictor of the GRN response is the interaction strength among network partners. By outlining the conditions that permit the operation of the GRN during NP maturation *in silico*, the model predicts and informs on cellular behaviors of the system *in vivo*.

Methods

Hill equations were used to model the signaling and transcription factor interaction networks. Within each equation, Hill constants were used to vary the strength of interaction between a molecule and its target substrate (e. g., interaction between a transcriptional regulator and its target gene; **Fig S1**). We first modeled the signaling network as it is responsible for the spatial regulation of the transcription factor network. Partial differential equation were used to model the synthesis, diffusion, degradation and interactions between FGF, WNT and RA signals. The output of the signaling network was then used as the input for the transcription factor network. This transcription factor network was solved using ordinary differential equations. We used MATLAB (MathWorks, Natick, MA) to solve the equations numerically and to plot the simulations. Partial differential equations were solved using *pdepe* solver and ordinary differential equations using *ode45* solver.

Hill equation based interaction model

In both networks, the rate of mRNA change was modeled using ordinary differential equations, and the rate of protein change was modeled using either ordinary differential equations for transcription factor or partial differential equations for signaling factors to accommodate diffusion [24-26]. These equations follow the general form;

mRNA dynamics:

$$\frac{\partial M}{\partial t} = \alpha_m H_1 - \beta_m M H_2$$

132 Protein dynamics for transcription factors:

133 $$\frac{\partial P}{\partial t} = \alpha_p M H_3 - \beta_p P H_4$$

134 Protein dynamics for signaling factors:

135 $$\frac{\partial P}{\partial t} = \alpha_p M H_3 - \beta_p P H_4 - \mu \frac{\partial \mathrm{P}}{\partial x^2}$$

136 ,where,

137 α_m = Transcription rate constant. α_p= Translation rate constant.

138 β_m= mRNA decay rate constant. β_p= protein decay rate constant.

139 M = mRNA concentration. P = protein concentration.

140 μ = diffusivity coefficient. x = spatial dimension.

141 H_1, H_2, H_3, H_4 are independent Hill functions that can describe one of four general types

142 of regulatory interaction between network components (see Supp. Methods): (1) inductive

143 interactions from one or multiple activators, (2) repressive interactions from one or multiple

144 repressors, (3) coordinated interactions between activators and repressors binding to separate

145 regulatory sites and (4) competitive interactions between activators or repressors binding to the

146 same regulatory sites. For each factor being modeled, we replaced H_1, H_2, H_3, and H_4 functions

147 with the appropriate equation that best describes the regulatory interactions observed

148 experimentally.

149

150 Equations modeling the signaling interactions network

151 Partial differential Hill equations were used to model FGF8, WNT8C and RA network of

152 interactions (**Fig 2A**). These interactions were modeled within a spatial maturation domain

153 restricted to a 2500 microns extending from the NMP zone to the anterior boundary of the last

154 formed somite (stage HH10-11 embryos; **Fig 1B, 2B**). This spatial maturation domain moves
155 caudally and in synchrony with the NMP zone during axial elongation, thus appearing stationary
156 with respect to the NMP zone (**Fig 2B**). When available, we used parameter values that have
157 been determined experimentally, within reported ranges. For parameters that have not been
158 determined experimentally (e.g., rates constants for mRNA and protein synthesis and
159 degradation), we used parameters values comparable to those used in other models [27-29].
160

161 **Fig 2. Signaling network output is determined by the strength of interactions between FGF,**
162 **WNT, and RA pathway components.** (**A**) FGF8, WNT8C and RA signaling pathway
163 interaction network based on [23]. Names in lower case indicate mRNA and upper case proteins
164 (FGF8 and WNT8C) or metabolites (RA). (**B**) The spatial maturation domain where the
165 signaling network operates extends from the NMP cells to the anterior boundary of the last
166 formed somite (vertical dashed lines; x-axes on graphs). The domain in the simulation has a
167 constant length maintained by a caudal movement that is equivalent to the rate of NMP cell
168 proliferation. Initially undifferentiated cells differentiate at a rate defined by the simulation (red
169 to green transition). (**C-E**) Representative FGF8 dominant (C), FGF-RA balance (D), and FGF-
170 RA switch (E) simulation profiles obtained using parameters shown in **Table 1**. Left graphs
171 shows the levels of the signaling molecules FGF8 (red), WNT8C (magenta) and RA (blue)
172 across the maturation domain at the end of the simulation (t=6000 min; arbitrary units AU).
173 Center and right graphs show heat maps of FGF8 (center) and RA (right) accumulation in the
174 maturation domain (x-axis) over time (y-axis). AU scale for FGF (maroon gradient) and RA
175 (blue gradient) are shown at right of graphs.
176

177 FGF8 PRODUCTION. *Fgf8* transcription is restricted to the NMP zone through positive
178 autoregulatory loops and inhibitory signals [30]. FGF8 indirectly stimulates its own transcription
179 by inducing transcription of *Nkx1.2*, *Cdx*, and WNT/ß-catenin pathway components [30]. RA
180 secreted from somites restricts *Fgf8* to the NMP zone in a concentration-dependent manner [13].
181 RA inhibition is excluded from NMP zone by CYP26A, an RA-catabolizing enzyme whose gene
182 is activated by FGF8 [31]. We simulated *Fgf8* positive autoregulatory loop by assuming a basal
183 exponential level of gene transcription, and its restriction to the caudal end of the spatial
184 maturation domain by allowing RA to decrease *Fgf8* transcription down to zero in a
185 concentration-dependent manner.

186 *Fgf8* mRNA transcripts have a long half-life of around 2 hours, persisting in cells long
187 after transcription has stopped [27, 32]. This long decay results in a graded distribution of
188 transcript in the spatial maturation domain, with cells proximal to the NMP zone retaining more
189 transcripts that more distal cells. This 2 hour half-life sets the rate constant of degradation to
190 around 0.006 min^{-1} (ln2/2h = 0.693/120min). As the average speed of axis elongation is 3μm/min
191 (from somite 5 to 11; [28]), the decay constant in the spatial maturation domain is 0.002 μm^{-1}.

192 FGF8 protein synthesis is dependent on the concentration of the *Fgf8* transcript within
193 each cell. As FGF8 is synthesized, it diffuses from producing cells at a rate that has been
194 determined experimentally to be around 2 μm^2/sec [33]. Due to this diffusion, the domain of
195 FGF protein signaling expands beyond the domain of *Fgf8* transcription.

196 Constant input: $F_0(x)$

197 $$F_0 = 0.06e^{-.002x} \quad (1)$$

198 *Fgf8* mRNA transcription: $F_m(t)$

199 $$\frac{\partial F_m}{\partial t} = \alpha_{Fm} F_0 \left(\frac{1}{(1+(R/R_{FR})^r)}\right) - \beta_{Fm} F_m \quad (2)$$

200 FGF8 translation: $F(x,t)$

201 $$\frac{\partial F}{\partial t} = \alpha_{Fp} F_m - \beta_{Fp} F - D_F \frac{\partial^2 F}{\partial x^2} \quad (3)$$

202 , where,

203 *Fgf8* mRNA transcription rate constant [27, 29] α_{Fm} = 1/min

204 *Fgf8* mRNA half-life [27] β_{Fm} = 0.006/min.

205 FGF8 translation rate constant [27] α_{Fp} = 0.3/min

206 FGF8 degradation rate constant [27] β_{Fp} = 0.005/min

207 FGF8 diffusion constant [33] D_F = 120 μm^2/min

208 Hill constant, *Fgf8* inhibition by RA R_{RF} (see **Table 1**)

209

Table 1. Examples of Hill constants combinations tested to investigate signaling dynamics behavior

Hill constants	I	II	III	IV	V	VI	VII	VIII
F_{FW} FGF dependent activation of *Wnt8c* transcription	10	10	10	10	10	10	10	10
F_{FR1} FGF dependent repression of *Raldh2* transcription	1	1	5	10	10	10	2	20
F_{FR2} FGF dependent activation of RA degradation (via CYP26A enzymes)	2	10	15	10	10	10	20	20
W_{WR} WNT dependent activation of *Raldh2* transcription	1	1	0.2	0.5	0.2	0.5	1	1
R_{RF} RA dependent repression of *Fgf8* transcription	10	1	0.2	0.1	0.3	0.45	1	20
R_{RR} RA dependent activation of *Raldh2* transcription	50	50	50	50	50	50	300	300
Outcome (t=6000 min)	FGF dominant	FGF-RA balance	FGF-RA switch				RA aberrant/ oscillatory	

210

211 WNT8C PRODUCTION. *Wnt8c* transcription is stimulated by FGF pathway activity and is

212 indirectly blocked by RA inhibiting *Fgf8* transcription [23]. In chick embryos, *Wnt8c* expression

213 domain significantly overlaps and extends far beyond *Fgf8* mRNA domain up to the last formed

214 somite (**Fig 1A**; [23, 34]), suggesting that very low levels of FGF8 can activate *Wnt8c* [23, 34].

215 By contrast, in the NMP zone, *Wnt8c* mRNA level are one-third of the *Fgf8* mRNA level [35],

216 which suggest that transcription rate constant of *Wnt8c* are low and saturate quickly [35]. Once

217 synthesized, WNT8C diffuse from its site of synthesis throughout the spatial maturation domain

218 at a low diffusion rate [36].

219 *Wnt8c* mRNA transcription: $W_m(t)$

220 $$\frac{\partial W_m}{\partial t} = \alpha_{Wm}\left(\frac{(F/F_{FW})^a}{(1+(F/F_{FW})^a)}\right) - \beta_{Wm}W_m \quad (4)$$

221 WNT8C translation: $W(x,t)$

222 $$\frac{\partial W}{\partial t} = \alpha_{Wp}W_m - \beta_{Wp}W - D_W\frac{\partial^2 W}{\partial x^2} \quad (5)$$

223 , where,

224 *Wnt8c* mRNA transcription rate constant [23, 34]	α_{Wm} = 0.1/min
225 *Wnt8c* mRNA half-life constant [23, 34]	β_{Wm} = 0.03/min
226 WNT8C translation rates constant [27]	α_{Wp} = 0.3/min
227 WNT8C degradation rates constant[27]	β_{Wp} = 0.01/min
228 WNT8C diffusion rate rates [36]	D_W = 10 μm^2/min
229 Hill constant, *Wnt8c* activation by FGF8	F_{FW} (see **Table 1**)

230

231 RA PRODUCTION. RA is synthesized in somites by the enzyme RALDH2 [37]. *Raldh2*

232 transcription is restricted to somites as this is the only region where activation by the WNT8C

233 pathway can overcome FGF8-dependent repression [23]. Parameters for RALDH2 production
234 and degradation were equivalent to those in other models [38]. We assumed that once RALDH2
235 is produced, RA synthesis initiates without delay. Once produced, RA diffuses into
236 undifferentiated neural and mesodermal tissues at an estimated rate of 18 μm^2/sec or about 1080
237 μm^2/min [38]. At the caudal end of the embryo, RA is degraded by the enzyme CYP26A, whose
238 transcription is under FGF8 regulation [21].

239 *Raldh2* mRNA transcription: $R_m(t)$

240 $$\frac{\partial R_m}{\partial t} = \alpha_{Rm}\left(\frac{(W/W_{WR})^a+(R/R_{RR})^a}{(1+(W/W_{WR})^a+(R/R_{RR})^a)}\right)\left(\frac{1}{(1+(F/F_{FR1})^r)}\right) - \beta_{Rm}R_m \quad (6)$$

241 RA production (as modeled by RALDH2 translation): $R(x,t)$

242 $$\frac{\partial R}{\partial t} = \alpha_{Rp}R_m - \beta_{Rp}R(1+\beta_{FR}\frac{(F/F_{FR2})^a}{(1+(F/F_{FR2})^a)}) - D_R\frac{\partial^2 R}{\partial x^2} \quad (7)$$

243 , where,

244 *Raldh2* mRNA transcription rate constant [27]	α_{Rm} = 1/min
245 *Raldh2* mRNA half-life constant [27]	β_{Rm} = 0.03/min
246 RALDH2 translation rates constant [27]	α_{Rp} = 0.3/min
247 RALDH2 degradation rates constant [27]	β_{Rp} = 0.025/min
248 RA estimated diffusion rate	D_R = 1200 μm^2/min
249 FGF dependent RALDH2 degradation constant	β_{FR} = 6/min
250 Hill constant, *Raldh2* induction by WNT8C	W_{WR} (see **Table 1**)
251 Hill constant, *Raldh2* induction by RA (autoregulation)	R_{RR} (see **Table 1**)
252 Hill constant, *Raldh2* repression by FGF8	F_{FR1} (see **Table 1**)
253 Hill constant, RA degradation by FGF8-induced CYP26A	F_{FR2} (see **Table 1**)

254

255 **Equations modeling the transcript factors interactions network**

256 We used differential equations to simulate the transcription factor network (**Fig 1C**), using as
257 inputs the FGF8, WNT8C and RA output levels obtained in the signaling simulation (represented
258 in the equations with the letters F, W and R, respectively). Network interactions are described in
259 the result section and are supported by previous publications (reviewed in [12]).

260 *T/Bra* mRNA: $T_m(t)$

261 (Synthesis activated by FGF8 and inhibited by SOX2.)

262 $$\frac{\partial T_m}{\partial t} = \alpha_{Tm}\left(\frac{(F/F_{FT})^a}{(1+(F/F_{FT})^a+(S/S_{ST})^r)}\right) - \beta_{Tm}T_m \quad (8)$$

263 T/BRA protein: $T(t)$

264 $$\frac{\partial T}{\partial t} = \alpha_{Tp}T_m - \beta_{Tp}T \quad (9)$$

265 *Sox2* mRNA: $S_m(t)$

266 (Synthesis activated by FGF8 and RA and inhibited by T/BRA.)

267 $$\frac{\partial S_m}{\partial t} = \alpha_{Sm}\left(\frac{(F/F_{FS})^a+(R/R_{RS})^a}{(1+(F/F_{FS})^a+(R/R_{RS})^a+(T/T_{TS})^r)}\right) - \beta_{Sm}S_m \quad (10)$$

268 SOX2 protein: $S(t)$

269 $$\frac{\partial S}{\partial t} = \alpha_{Sp}S_m - \beta_{Sp}S \quad (11)$$

270 *Nkx1.2* mRNA: $NK_m(t)$

271 (*Nkx1.2* is activated by WNT8C and inhibited by a CDX4-dependent factor X and NKX1.2.)

272 $$\frac{\partial NK_m}{\partial t} = \alpha_{NKm}\left(\frac{(W/W_{WNK})^a}{(1+(W/W_{WNK})^a+(NK/NK_{NKNK})^r+(X/X_{XNK})^r)}\right) - \beta_{NKm}NK_m \quad (12)$$

273 NKX1.2 protein: $NK(t)$

274 $$\frac{dNK}{dt} = \alpha_{NKp}NK_m - \beta_{NKp}NK \quad (13)$$

275 *Cdx4* mRNA: $C_m(t)$

(*Cdx4* is induced by FGF8 and WNT8C and inhibited by a PAX6-dependent factor Y.)

$$\frac{\partial C_m}{\partial t} = \alpha_{Cm}\left(\frac{(F/F_{FC})^a+(W/W_{WC})^a}{(1+(F/F_{FC})^a+(W/W_{WC})^a+(Y/Y_{YC})^r)}\right) - \beta_{Cm}C_m \quad (14)$$

CDX4 protein: $C(t)$

$$\frac{\partial C}{\partial t} = \alpha_{Cp}C_m - \beta_{Cp}C \quad (15)$$

Factor *X* mRNA: $X_m(t)$

(Factor *X* is induced CDX4. We have assumed that *X* is inhibited by high FGF8 levels since repression of *Nkx1.2* by CDX4-dependent Factor X is not effective in NMP zone.)

$$\frac{\partial X_m}{\partial t} = \alpha_{Xm}\left(\frac{(C/C_{CX})^a}{(1+(C/C_{CX})^a+(F/F_{FX})^r)}\right) - \beta_{Xm}X_m \quad (16)$$

X protein: $X(t)$

$$\frac{\partial X}{\partial t} = \alpha_{Xp}X_m - \beta_{Xp}X \quad (17)$$

Pax6 mRNA: $P_m(t)$

(*Pax6* is induced by CDX4 and RA working cooperatively, and is inhibited by NKX1.2)

$$\frac{\partial P_m}{\partial t} = \alpha_{Pm}\left(1+\frac{(C/C_{CP})^a}{(1+(C/C_{CP})^a+(NK/NK_{NKP})^r)}\right)\left(\frac{(R/R_{RP})^a}{(1+(R/R_{RP})^a)}\right) - \beta_{Pm}P_m \quad (18)$$

PAX6 protein: $P(t)$

$$\frac{\partial P}{\partial t} = \alpha_{Pp}P_m - \beta_{Pp}P \quad (19)$$

Factor *Y* mRNA: $Y_m(t)$

(Synthesis activated by PAX6, and inhibited by FGF8.)

$$\frac{\partial Y_m}{\partial t} = \alpha_{Xm}\left(\frac{(P/P_{PY})^a}{(1+(P/P_{PY})^a+(F/F_{FY})^r)}\right) - \beta_{Ym}Y_m \quad (20)$$

Y protein: $Y(t)$

$$\frac{\partial Y}{\partial t} = \alpha_{Yp}Y_m - \beta_{Yp}Y \quad (21)$$

Ngn2 mRNA: $N_m(t)$

297 (Synthesis activated by PAX6 and inhibited by factor X.)

298 $$\frac{\partial N_m}{\partial t} = \alpha_{Nm}\left(\frac{(P/P_{PN})^a}{(1+(P/P_{PN})^a+(X/X_{XN})^r)}\right) - \beta_{Nm}N_m \quad (22)$$

299 Name definition and values for the Hill constants used in the transcription factor network are
300 found in **Table 2**. For all these transcription factors, the rate constants of mRNA and protein
301 synthesis and degradation have not been determined experimentally. Hence, all the values are
302 kept similar based on values used in published models [27, 29]. The only exception was CDX4,
303 as CDX proteins are known to have increased stability [39].

304 Constant for mRNA synthesis/degradation: α_{im} = 1/ min β_{im}= 0.03/ min

305 Constant for protein synthesis/degradation: α_{ip} = 1/ min β_{ip}= 0.2/ min

306 CDX4 constant for protein synthesis/degradation: α_{Cp} = 1/ min β_{Cp}= 0.05/ min

307

Table 2: Hill constant for correct spatiotemporal distribution of cellular states.

Hill constants	Description	Value*
F_{FT}	FGF8 dependent activation of *T*	10
F_{FS}	FGF8 dependent activation of *Sox2*	50
F_{FC}	FGF8 dependent activation of *Cdx4*	5
F_{FX}	FGF8 dependent repression of *X*	1
F_{FY}	FGF8 dependent repression of *Y*	1
W_{WN}	WNT8C dependent activation of *Nkx1.2*	10
W_{WC}	WNT8C dependent activation of *Cdx4*	10
S_{ST}	SOX2 dependent repression of *T*	2
T_{TS}	T dependent repression of *Sox2*	20
N_{NN}	NKX1.2 dependent repression of *Nkx1.2*	100

N_{NP}	NKX1.2 dependent repression of *Pax6*	20
C_{CX}	CDX4 dependent activation of *X*	10
C_{CP}	CDX4-RA complex dependent activation of *Pax6*	10
R_{RS}	RA dependent activation of *Sox2*	1
R_{RP}	RA dependent activation of *Pax6*	10
X_{XN}	X dependent repression of *Nkx1.2*	1
X_{XN2}	X dependent repression of *Ngn2*	1
P_{PY}	PAX6 dependent activation of *Y*	5
P_{PN2}	PAX6 dependent activation of *Ngn2*	20
Y_{YC}	Y dependent repression of *Cdx4*	5
*Correct spatiotemporal distribution of cellular states was also obtained when individual values are increased or decreased by 30%		

Results

FGF-WNT-RA signaling interaction network can drive signaling switch

In order to model the transcription factor network responsible for spinal cord cell maturation (**Fig 1C**), we first simulated the signaling dynamics between FGF, WNT and RA driving the system [13, 23]. Although several partially redundant FGF and WNT factors are transcribed within and around the caudal neural plate [23, 40], for simplicity, we focused on the factors shown to have the most influence on the system, FGF8 and WNT8C [23]. *Fgf8* is transcribed in the caudal stem zone (**Fig 1A**), where it activates *Wnt8c* transcription [23] and represses RA activity via two mechanisms: by inhibiting transcription of the RA synthesis enzyme *Raldh2* and activating

319 transcription of the RA degradation enzyme *Cyp26a* [21]. FGF8 inhibition of RA production is
320 circumvented rostrally by *Fgf8* mRNA decay [32] and by WNT8C, which stimulates RA
321 production by outcompeting FGF8-mediated *Raldh2* repression [23]. Once *Raldh2* induction has
322 occurred in nascent somites, its expression is maintained through unknown mechanisms even in
323 the absence of WNT activity [23]. For simplification, our model assumes that RA maintains
324 *Raldh2* transcription through positive autoregulation [41]. RA produced by somites then diffuses
325 caudally and inhibit *Fgf8* transcription [21, 42]. These interactions give rise to an extended
326 negative feedback loop between FGF and RA (**Fig 2A**).

327 Cell proliferation in the stem zone extend the vertebrate body axis caudally by producing
328 the cells that, upon maturation, give rise to the trunk and tail [8]. To simulate the tissue's caudal
329 ward movement, the signaling interactions were confined to a caudally moving spatial
330 maturation domain of constant length extending rostrally from the stem cell zone to the anterior
331 boundary of the most recently formed somite (**Fig 2B**). Thus, from the perspective of the caudal
332 end, the moving spatial maturation domains appears stationary. To simulate the interactions
333 between signaling factors, we used partial differential equations that integrated synthesis,
334 degradation, and diffusion constant through interaction parameters or Hill constants. The Hill
335 constant of a given reaction is the concentration of a factor involved in transcription or signaling
336 at which the rate of reaction regulated by the factor is half of the maximum possible rate. Hence,
337 Hill constant is inversely related to the affinity of a factor for its target and can act as a measure
338 of factor's interaction strength (**Fig S1**).

339 To understand the possible behaviors that could originate from the extended FGF-WNT-
340 RA network, we analyzed the system's output after systematically changing the signaling inputs
341 and the strength of interaction between components (strong Hill constant =0.1 to weak Hill

342 constant =100). By varying the interaction strength between FGF, WNT and RA components we
343 obtained various temporal signaling information profiles that we grouped into four broad
344 behaviors: FGF-dominance, FGF-RA balance, FGF-RA switch, and RA aberrant/oscillatory.

345 *FGF8 dominance*: In a system where FGF8 repression of *Raldh2* transcription outweighs
346 RA repression of *Fgf8* transcription, the interactions do not result in appreciable RA production
347 (e. g., **Table 1-I; Fig 2C, Fig S2A**). Such a system would lead to maintenance of pluripotent
348 stem progenitor cells without differentiation.

349 *FGF8-RA balance*: FGF8, WNT8C and RA signaling domains balance each other and
350 settle on a stable steady state profile (**Table 1-II; Fig 2D, Fig S2A, B**). Such steady state is
351 achieved when the activating and repressive interactions of the system reach an equilibrium. In
352 these conditions, the regions of FGF8 and RA activities are restricted to domains that maintain
353 the same distance from one.

354 *FGF-RA switch*: The most interesting behavior obtained from simulation is where the
355 system starts with an *Fgf8* mRNA gradient and ends with RA activity gradient over the entire
356 spatial domain (**Table 1-III; Fig 2E, Fig S2A**). This behavior simulates a system that starts with
357 a caudally located stem cell zone and a field of undifferentiated cells that is gradually converted,
358 in a rostral to caudal direction, to a field of differentiate cells. Significantly, this differentiation
359 process is the mechanism by which axial elongation is thought to cease in embryos [31, 43]. The
360 rate at which the FGF8-to-RA transition occurs, and hence differentiation, is modulated by the
361 strength of mutually repressive FGF-RA interactions (**Table 1-IV through VI**; **Fig 3**).

362

363 **Fig 3. RA inputs strength determine FGF-RA switch rate of conversion.** The strength by
364 which WNT8C stimulates (W_{WR}) and FGF8 represses (R_{RF}) *Raldh2* transcription determines
365 RA's spatial profile over time (x and y axes, respectively). (**A**) Fast FGF-RA switch (t<1500
366 min) results from relatively moderate activation and very strong repression inputs (W_{WR}=0.5,
367 R_{RF}=0.1). (**B**) Intermediate FGF-RA switch (t<3000 min) results from relatively strong
368 activation and moderate repression inputs (W_{WR}=0.2, R_{RF}=0.3). (**C**) Slow FGF-RA switch
369 (t<5500 min) results from moderate activation and repression inputs (W_{WR}=0.5, R_{RF}=0.45). FGF
370 and RA heat map scale is shown on the right (arbitrary units; A. U.).

371

372 *RA aberrant/oscillatory*: Some parameters in the FGF-WNT-RA interaction system lead
373 to an oscillation in RA levels that did not match the behavior of the system *in vivo*. These
374 oscillations occurred when Hill constants for RA inputs were weak, particularly for the RA-
375 dependent autoregulation of *Raldh2* production (**Table 1-VII, VIII**; **Fig S3**). In some cases, the
376 system produced a discrete burst of RA at the position where the FGF-RA switch was observed,
377 to then return to produce FGF (**Table 1-VII**; **Fig S3A**). In other cases, the burst of RA separated
378 the caudal area of FGF production from a rostral area where FGF and RA production alternated
379 in an oscillatory manner (**Table 1-VIII**; **Fig S3B**).

380 Altogether, our results show that the FGF8-WNT8C-RA interaction network postulated
381 by Olivera-Martinez and colleagues [23] can indeed give rise to a signaling switch that travels
382 caudally during the elongation of the embryonic axis. The behavior of the switch depends on
383 several interaction parameters that, in coordination, regulate the position and size of the region of
384 cell differentiation.

385

386 ## FGF-WNT-RA signaling switch and transcription factor network
387 ## establish areas of pluripotency, early and late differentiation

388 To simulate the dynamics of the transcription factor network, we integrated the transcription (**Fig**
389 **1C**) and signaling (**Fig 2A**) networks into a single supra-network (**Fig 4A**). We then used the
390 FGF-RA balance profile output as the input for the system (**Fig 2D, 4B**), as it most closely
391 resembles the distribution of signaling activity during the steady state period of embryo growth
392 (**Fig 1A**). In this simulation, we followed the transcriptional profile of cells as they are born
393 caudally at t=0 and at subsequent times are displaced rostrally by the appearance of new cells.
394 During their rostral displacement, cells move away from the stem cell zone and the source of
395 FGF and WNT production (**Fig 4C**). As FGF/WNT level decrease, RA levels increase following
396 the FGF-RA balance profile simulation (**Fig 2D, 4B**). These changes in spatial signal
397 information are the drivers for transcription factor expression. Since the cells are arranged
398 spatially from caudal to rostral in order of birth, the temporal changes in transcription factors
399 give rise to spatial changes in profiles.

400

401 **Fig 4. Strength of interactions between transcription factors determine the response of the**
402 **network to signal information.** (**A**) Integrated transcription and signaling interaction network,
403 including hypothetical factors X and Y, predicted from experimental data from reference [12].
404 (**B**) Reference FGF-RA switch input used for simulations (from **Fig 2D**). (**C**) Location of
405 reference cell (circle) within the spatial maturation domain of signaling activity (vertical dashed
406 lines). Cell remains in the location where it was born as the spatial maturation domain is

407 displaced caudally (as in **Fig 2B**). (**D-F**) Transcription profile of cell with all interactions equally
408 moderate (D; Hill constants=20), equally strong (E; Hill constants=2), and variable (F; as defined
409 in **Table 2**). Output of simulation in F most closely resembles the staggered distribution of
410 transcription factors observed in embryos (**Fig 1B**; [12]). Colored bars at the bottom of each
411 graph represent the spatial domain of gene transcription: *Sox2* in dark orange; *T/Bra* in dark blue;
412 *Nkx1.2* in light orange; *Cdx4* in purple; *Pax6* in light blue; and *Ngn2* in maroon.

413

414 The transcription output of the system depends on signaling inputs and transcription
415 factor interactions. Signals regulate the transcription factor network at two distinct key points.
416 The first point of regulation is towards the caudal end of the embryo, where FGF8 and WNT8C,
417 alone or in combination, are required for *T (Bra), Sox2, Nkx1.2* and *Cdx4* transcription [14, 44-
418 48]. Independently of signaling inputs, *Nkx1.2* transcription is negatively regulated by CDX4 and
419 its own protein product [12, 46]. The second point of regulation is towards the rostral end of the
420 neural plate, where RA cooperates with CDX4 to activate the early differentiation gene *Pax6*
421 [12, 49]. *Pax6* is also negatively regulated by NKX1.2 [12, 50]. In contrast, transcription of late
422 differentiation gene *Ngn2* is activated by PAX6 and repressed by CDX4 [12, 22]. Given that
423 CDX4 is an activator and not a repressor [51], our model invokes two putative repressors *X* and
424 *Y* to mediate the repressive activity of CDX4 on *Nkx1.2* and *Ngn2* [12]. These hypothetical
425 repressors are assumed to be inhibited by FGF8 [12].

426 Signal and transcription factor network were able to generate correct gene transcription
427 profile in many but not all instances (**Fig 4D-F**), indicating that only under certain parameter
428 restrictions could the network recapitulates embryonic events. In principle, the spatial dynamics
429 of the signal interactions network should be sufficient to activate transcription factor network

430 components in the correct spatiotemporal sequence: high FGF caudally would promote
431 pluripotency while high RA rostrally would promote differentiation, with cross-repressive
432 interaction between pathways maintaining the domains separate at opposite ends of the tissue.
433 However, if all the interactions in the network are equally moderate (Hill constants =20, **Fig 4D**)
434 or equally strong (Hill constants =2, **Fig 4E**), then the network does not result in the proper
435 spatial resolution of temporal states. In both cases, transcription of the mesoderm marker *T/Bra*
436 is not restricted to the caudal end, but instead, it is detected throughout the caudal two thirds of
437 the tissue, partially overlapping with *Pax6* and *Ngn2* gene transcripts (**Fig 4D, E**). Only a subset
438 of interaction strengths give rise to correct spatial order of identities (**Table 2; Fig 4F**). The
439 values of the interactions strengths that generate proper spatial distribution of transcripts could
440 be increased or decreased by 30%. These values define a parametric space where the model is
441 operational and highlights its robustness **(Fig S4).** These results suggest that signaling inputs
442 encodes the information required for specifying different cell maturation states, but that it is the
443 transcription factor network what determines the spatial distribution and organization of
444 maturation states cell along the caudal-to-rostral length of the tissue.

445

446 The transcription network executes the spatiotemporal information 447 provided by the signaling factor network

448 To further evaluate the contribution of signaling and transcription factors networks on cell
449 maturation events, we tested the effect of disrupting individual network nodes on transcription
450 readouts. First, we tested the response of the transcription network to signaling noise. In
451 simulations, both periodic disturbance (**Fig 5A**) and random noise (**Fig 5B**) were well tolerated

452 by the transcription network without any distortions in the spatiotemporal resolution of the
453 cellular states. Unexpectedly, introduction of random noise resulted in better separation of
454 maturation (Cdx4$^+$, Pax6$^+$, Ngn2$^-$) and late differentiation (Cdx4$^-$, Pax6$^+$, Ngn2$^+$) states (**Fig. 4F,**
455 **5B**). This suggest that transcription network has built in robustness to extrinsic disturbances.
456
457 **Fig 5. Transcription factor network is resilient to small and moderate alterations in**
458 **signaling information.** (**A, B**) Transcription factor output is not affected by oscillatory (A) or
459 random noise (B) in signaling inputs, as outputs are comparable to those obtained in conditions
460 without noise (Fig 4F). (**C, D**) Large changes in signaling input such as discreet Boolean (C) and
461 linear gradient (D) changes transcription factor expression domains.
462

463 Next, we evaluated the role of signaling gradients in determining the spatiotemporal
464 resolution of downstream targets' transcriptional domains. Replacing the exponential gradient of
465 the signaling factors with a Boolean switch (**Fig 5C**) or a linear gradients (**Fig 5D**), resulted in
466 loss of proper resolution of transition zones. Thus, changes in the spatial information contained
467 in the signaling network changes the transcription network readouts. This confirms that the
468 spatial information is encoded in the signaling and not in transcription factor network.

469 We previously proposed a central role of CDX4 in regulating maturation of NPs in the
470 pre-neural tube. To theoretically test CDX4 role in transcription network regulation, we
471 removed, increased or introduced noise to *Cdx4* transcription and evaluated the network's
472 transcription profile output (**Fig 6**). When *Cdx4* was removed from the simulation, *Nkx1.2*
473 transcription expanded rostrally, overlapping significantly with the expression of differentiation
474 markers *Pax6* and *Ngn2* (**Fig 6A**). This phenomenon is opposite to what is observed

475 experimentally, were downregulation of CDX4 activity using an ENRCDX4 repression construct
476 results in downregulation of *Nkx1.2* [12] (discussed below). Conversely, when the levels of *Cdx4*
477 were increased in the simulation, *Nkx1.2* expression domain shifted caudally, away from *Pax6*
478 expression domain, and rostral cells did not activate the late differentiation gene *Ngn2* (**Fig 6B**),
479 in agreement with experimental results [12]. Thus, removing or increasing *Cdx4* transcription
480 affects the spatial relationship between early specification gene *Nkx1.2* and neural differentiation
481 gene *Ngn2*, indicating that CDX4 function in the network is key to establish a transition zone
482 between pluripotency and differentiation states. This function of CDX4 is robust, as introduction
483 of transcriptional noise still produce the expected gene expression profile with only minute
484 changes in the position of boundary transitions (<+/-30µm; **Fig 6C)**. Thus, with the one
485 exception of Cdx4 removal discussed below, our simulation generally agrees with our *in vivo*
486 observed role of CDX4 in driving NP maturation during early spinal cord development.

487

488 **Fig 6. CDX4 is necessary for proper interpretation of signaling inputs by the transcription**
489 **factor network.** (**A**) Compared to control simulation (Fig 4F), loss of *Cdx4* expression causes a
490 large rostral expansion of *Nkx1.2* domain, a small reduction in *Pax6* domain and a large caudal
491 expansion in *Ngn2* domain. These changes results in the overlap of stem and differentiation gene
492 expression domains. (**B**) Overexpression of *Cdx4* reduces *Nkx1.2* and eliminates *Ngn2*
493 expression domains, effectively expanding the early and eliminating the late differentiation
494 zones. (**C**) Introduction of random noise in *Cdx4* transcriptional noise has insignificant effects on
495 the system's spatial expression profiles. In the expression profile bars at the bottom of the
496 graphs, white and black rectangles indicate loss and gain of gene transcription, respectively.

497

Discussion

Signaling factor simulation recapitulates signaling dynamics observed in natural systems

Our simulations describe the possible behaviors the FGF8-WNT8C-RA system can exhibit under various interaction conditions (**Fig 2**). With small variations in interactions' strength, the system can model behaviors associated with different stages of axial tissue development. In a system where the FGF's activity dominates over RA's activity, the simulation most closely resembles the neural tissue at early stages of axial extension, whereas in a system where FGF activity balances that of RA, the simulation resembles the maturation of spinal cord cell that occurs during axial elongation. In contrast, a switch in the system from FGF to RA most closely resembles the processes occurring during termination of body axis extension [9, 28]. Significantly, when the interactions between FGF and RA components are weak, the system oscillates, resembling the oscillations observed between FGF/WNT and the Notch signaling pathway during the process of paraxial mesoderm segmentation [52]. Thus, with small modifications in signal components interaction, one can observe large changes in the behavior of the system equivalent to the changes normally observed in the tissues emerging from the tailbud during axial elongation, the paraxial mesoderm and spinal cord.

We propose a model of vertebrate body extension where modulation of interaction strength between different components of the system (e.g., transcriptionally, post-transcriptionally or epigenetically), could regulate the spatiotemporal dynamics involved in

519 vertebrate body extension. In this model, the time at which the system transitions from FGF
520 dominant, to FGF-RA balance, to RA switch respectively determine the time of tissue induction,
521 elongation and termination. For example, a long period in which the FGF8-RA balance system is
522 operational could explain the elongated axis of vertebrates such as snakes; as long as the FGF8-
523 RA balance system remains operational, the caudal progenitor/stem cell pool will continue to
524 generate tissue and extend the axis. In this scenario, the time at which RA takes over the system
525 to initiate progenitor cell differentiation will determine the axial body length, with a fast FGF-
526 RA switch resulting in a shorter body axis and vice versa.

527

528 Transcription network simulations recapitulate the cell state
529 transitions observed in the caudal neural plate

530 Results from simulations support a role for CDX in coordinating upstream signaling factors with
531 downstream transcription network components involved in spinal cord neural maturation. In the
532 present model, CDX4 functions to separate caudal stem cell populations (*Nkx1.2*$^{+}$ *Pax6*$^{-}$ *Ngn2*$^{-}$)
533 from rostral differentiating cells (*Nkx1.2*$^{-}$ *Pax6*$^{+}$ *Ngn2*$^{+}$) by establishing a transition zone. This is
534 achieved by CDX4 repressing the bipotency gene *Nkx1.2* and the late differentiation gene *Ngn2*,
535 and by activating the early differentiation gene *Pax6*. In simulations, high levels of *Cdx4*
536 transcription resulted in downregulation of CDX4 repressed genes (**Fig 6B**): *Nkx1.2* transcription
537 domain shifted caudally and *Ngn2* transcription was lost. In these conditions, only the caudal
538 expression of *Nkx1.2* was retained due to its high dependence on WNT stimulation [46].
539 Increasing *Cdx4* transcription did not affect the expression domain of *Pax6,* as transcription of
540 this gene is also dependent on RA secreted from somites [12, 49]. Together, the changes in

541 *Nkx1.2* and *Ngn2* transcription induced by CDX4 overexpression effectively increase the size of
542 the transition zone. The same way that premature activation of differentiation signals has been
543 predicted to cause shortening of the embryonic axis [31], a greater separation of stem cell and
544 differentiation signals is predicted to cause axial lengthening. These predictions would need to be
545 tested experimentally.

546 Significantly, results obtained by simulating loss of *Cdx4* activity (**Fig 6A**) did not fully
547 match experiments done *in vivo*. With respect to differentiation genes, the network recapitulates
548 the *in vivo* results: *Pax6* transcription was not affected due to dependence of this gene on RA
549 [12, 49], whereas *Ngn2* transcription was upregulated because this gene is normally repressed by
550 CDX4 [12]. In contrast, with respect to the NMP marker *Nkx1.*2, loss of *Cdx4* caused an anterior
551 expansion of *Nkx1.2* expression domain that was not observed experimentally. This discrepancy
552 can be attributed to the use of a dominant negative form of CDX4 instead to knockout allele to
553 downregulate the activity of this gene *in vivo* (ENRCDX4; [12]). Dominant-negative ENRCDX4
554 works by outcompeting endogenous CDX4 from binding to its target genes and repressing their
555 transcription [53]. This approach is different than not having CDX4 protein altogether (e. g,
556 through deletion of the gene). Given that our model simulates the loss of CDX4 function and not
557 the active repression of its downstream target genes, this providing a possible explanation for the
558 observed discrepancies between experimental systems. It is also possible that our current
559 understanding of the transcription factor network is incomplete. These two possible explanations
560 are not mutually exclusive, and could be resolved with additional experiments. While additional
561 experiments will be required to fully understand CDX4 function in the NMP zone, even with its
562 limitations, the proposed transcription factor network supports a key role for CDX4 in the

563 segregation of cell states in the nascent spinal cord, providing a robust mechanisms for the
564 progressive maturation of cells during axial elongation.

565

566 Future perspectives

567 Although the integrated signaling and transcription factor network model presented here
568 provides key information on the transition state drivers underlying neuronal cell maturation, it is
569 clear from experimental and modelling data that the model is far from complete. One key
570 component missing from the model is the feedback control that transcription factors have over
571 the signaling network. Chromatin immunoprecipitation studies comparing anterior versus
572 posterior portions of mouse embryos have shown that CDX2 can regulate *Wnt5a*, *Rspo3* (a WNT
573 pathway component), *Fgf4* and *Fgf8*, indicating that CDX2 contributes to signaling factor
574 regulation and axial growth [54]. Similarly, CDX binding sites are present in *Radh2* intronic
575 enhancer are sufficient to drive reporter gene expression in the caudal end of embryos [55].
576 Currently, however, lack of quantitative data precluded the incorporation of feedback activities
577 into an integrated network model.

578 Our modeling results also highlights the importance of signaling factor regulation by
579 components external to the signaling pathways. For example, our model shows that maintenance
580 of RA production is critical for the behavior of the system, as weakening of the Hill constant
581 regulating RA-dependent autoregulation of *Raldh2* production causes the system to transition
582 from balanced to oscillatory (**Table 1-VII, VIII**; **Fig S3**). While, for simplification purposes we
583 assumed that Raldh2 maintenance is dependent or RA, it is likely to be dependent on
584 transcription factors, some of which are part of our transcription network (e.g. CDX; [55]).

585 Understanding the effect that transcription factor network components have over the signaling
586 network will be important for understanding the later stages in neural cell maturation and their
587 subsequent differentiation.

588

589 # Author contributions

590 P.J. and I.S. designed the experiments. P.J. derived the mathematical equations, coded the
591 simulation and performed experiments. P.J. and I.S. analyzed the results and wrote the
592 manuscript.

593

594 # Competing interests

595 No competing interest declared.

596

597 # Acknowledgements

598 We thank Dr. Donald DeAngelis for guidance and for sharing his mathematical expertise, and
599 members of the Skromne lab for intellectual discussion. We also thank Dr. K. G. Story (U
600 Dundee, UK), Dr. M. Gouldin (Salk Institute, USA). Dr. F. Medeville (CBI, France), Dr. S.
601 Mackem (NCI, USA), Dr. Y. Marikawa (U Hawaii, USA), Dr. A. V. Morales (Cajal Institute,
602 Spain) and Dr. B. Novitch (UCLA, USA) for generously providing plasmids.

603

604 # Funding

605 P. J. was supported by Sigma XI GIAR. I. S. was supported by University of Richmond School
606 of Arts and Sciences and by the National Science Foundation (IOS-1755386).

607

608 # References

609 1. Housden BE, Perrimon N. Spatial and temporal organization of signaling pathways. Trends
610 Bioch Sci. 2014;39: 457-464. doi: 10.1016/j.tibs.2014.07.008.
611 2. Egli D, Birkhoff G, Eggan K. Mediators of reprogramming: transcription factors and
612 transitions through mitosis. Nat Rev Mol Cell Biol. 2008;9:505-516. doi: 10.1038/nrm2439.
613 3. Basson MA. Signaling in cell differentiation and morphogenesis. CSH Persp Biol. 2012;4:
614 a008151. doi: 10.1101/cshperspect.a008151.
615 4. Perrimon N, Pitsouli C, Shilo BZ. Signaling mechanisms controlling cell fate and embryonic
616 patterning. CSH Persp Biol. 2012;4: a005975. doi: 10.1101/cshperspect.a005975.
617 5. Zaret KS, Watts J, Xu J, Wandzioch E, Smale ST, Sekiya T. Pioneer factors, genetic
618 competence, and inductive signaling: programming liver and pancreas progenitors from the
619 endoderm. CSH Symp Quant Biol. 2008;73: 119-126. doi: 10.1101/sqb.2008.73.040.
620 6. Zaret KS, Carroll JS. Pioneer transcription factors: establishing competence for gene
621 expression. Genes Dev. 2011;25: 2227-2241. doi: 10.1101/gad.176826.111.
622 7. Halfon MS, Carmena A, Gisselbrecht S, Sackerson CM, Jimenez F, Baylies MK, et al. Ras
623 pathway specificity is determined by the integration of multiple signal-activated and tissue-
624 restricted transcription factors. Cell. 2000;103: 63-74. doi: 10.1016/s0092-8674(00)00105-7.
625 8. Henrique D, Abranches E, Verrier L, Storey KG. Neuromesodermal progenitors and the
626 making of the spinal cord. Development. 2015;142: 2864-2875. doi: 10.1242/dev.119768.

627 9. Wilson V, Olivera-Martinez I, Storey KG. Stem cells, signals and vertebrate body axis
628 extension. Development. 2009;136: 1591-1604. doi: 10.1242/dev.021246.
629 10. Gouti M, Metzis V, Briscoe J. The route to spinal cord cell types: a tale of signals and
630 switches. Trends Genetics. 2015;31: 282-289. doi: 10.1016/j.tig.2015.03.001.
631 11. Gouti M, Tsakiridis A, Wymeersch FJ, Huang Y, Kleinjung J, Wilson V, et al. In vitro
632 generation of neuromesodermal progenitors reveals distinct roles for Wnt signalling in the
633 specification of spinal cord and paraxial mesoderm identity. PLoS Biology. 2014;12:
634 e1001937. doi: 10.1371/journal.pbio.1001937.
635 12. Joshi P, Darr AJ, Skromne I. CDX4 regulates the progression of neural maturation in the
636 spinal cord. Dev Biol. 2019; 449: 132-142. doi: 10.1016/j.ydbio.2019.02.014.
637 13. Diez del Corral R, Olivera-Martinez I, Goriely A, Gale E, Maden M, Storey K. Opposing
638 FGF and retinoid pathways control ventral neural pattern, neuronal differentiation, and
639 segmentation during body axis extension. Neuron. 2003;40: 65-79. doi:: 10.1016/s0896-
640 6273(03)00565-8.
641 14. Delfino-Machin M, Lunn JS, Breitkreuz DN, Akai J, Storey KG. Specification and
642 maintenance of the spinal cord stem zone. Development. 2005;132: 4273-4283. doi:
643 10.1242/dev.02009.
644 15. Gouti M, Delile J, Stamataki D, Wymeersch FJ, Huang Y, Kleinjung J, et al. A Gene
645 Regulatory Network Balances Neural and Mesoderm Specification during Vertebrate Trunk
646 Development. Dev Cell. 2017;41: 243-261. doi: 10.1016/j.devcel.2017.04.002.
647 16. Koch F, Scholze M, Wittler L, Schifferl D, Sudheer S, Grote P, et al. Antagonistic Activities
648 of Sox2 and Brachyury Control the Fate Choice of Neuro-Mesodermal Progenitors. Dev Cell.
649 2017;42: 514-526. doi: 10.1016/j.devcel.2017.07.021.

650 17. Takemoto T, Uchikawa M, Yoshida M, Bell DM, Lovell-Badge R, Papaioannou VE, et al.
651 Tbx6-dependent Sox2 regulation determines neural or mesodermal fate in axial stem cells.
652 Nature. 2011;470:394-398. doi: 10.1038/nature09729.
653 18. Yamaguchi TP, Takada S, Yoshikawa Y, Wu N, McMahon AP. T (Brachyury) is a direct
654 target of Wnt3a during paraxial mesoderm specification. Genes Dev. 1999;13:3185-3190.
655 doi: 10.1101/gad.13.24.3185.
656 19. Herrmann BG, Labeit S, Poustka A, King TR, Lehrach H. Cloning of the T gene required in
657 mesoderm formation in the mouse. Nature. 1990;343:617-622. doi: 10.1038/343617a0.
658 20. Pituello F, Medevielle F, Foulquier F, Duprat AM. Activation of Pax6 depends on
659 somitogenesis in the chick embryo cervical spinal cord. Development. 1999;126: 587-596.
660 21. Diez del Corral R, Storey KG. Opposing FGF and retinoid pathways: a signalling switch that
661 controls differentiation and patterning onset in the extending vertebrate body axis.
662 BioEssays. 2004;26: 857-869. doi: 10.1002/bies.20080.
663 22. Bel-Vialar S, Medevielle F, Pituello F. The on/off of Pax6 controls the tempo of neuronal
664 differentiation in the developing spinal cord. Dev. Biol. 2007;305: 659-673. doi:
665 10.1016/j.ydbio.2007.02.012.
666 23. Olivera-Martinez I, Storey KG. Wnt signals provide a timing mechanism for the FGF-
667 retinoid differentiation switch during vertebrate body axis extension. Development.
668 2007;134: 2125-2135. doi: 10.1242/dev.000216.
669 24. Sherman MS, Cohen BA. Thermodynamic state ensemble models of cis-regulation. PLoS
670 Comp. Biol. 2012;8: e1002407. doi: 10.1371/journal.pcbi.1002407.
671 25. Santillan M. On the Use of the Hill Functions in Mathematical Models of Gene Regulatory
672 Networks. Math. Mod. Nat. Phenom. 2008;3: 85-97. doi: 10.1051/mmnp:2008056.

673 26. Shi W, Ma W, Xiong L, Zhang M, Tang C. Adaptation with transcriptional regulation. Sci
674 Rep. 2017;7: 42648-42659. doi: 10.1038/srep42648.
675 27. Tiedemann HB, Schneltzer E, Zeiser S, Hoesel B, Beckers J, Prezmeck GK, et al. From
676 dynamic expression patterns to boundary formation in the presomitic mesoderm. PLoS Comp
677 Biol. 2012;8: e04379. doi: 10.1371/journal.pcbi.1002586.
678 28. Denans N, Iimura T, Pourquie O. Hox genes control vertebrate body elongation by collinear
679 Wnt repression. eLife. 2015;4: e04379. doi: 10.7554/eLife.04379.
680 29. Kiparissides A, Koutinas M, Moss T, Newman J, Pistikopoulos EM, Mantalaris A.
681 Modelling the Delta1/Notch1 pathway: in search of the mediator(s) of neural stem cell
682 differentiation. PLoS One. 2011;6: e14668. doi: 10.1371/journal.pone.0014668.
683 30. Diez del Corral R, Morales AX. The multiple roles of FGF signaling in the developing spinal
684 cord. Front Cell Dev Biol. 2017;5: 58. doi: 10.3389/fcell.2017.00058
685 31. Olivera-Martinez I, Harada H, Halley PA, Storey KG. Loss of FGF-dependent mesoderm
686 identity and rise of endogenous retinoid signalling determine cessation of body axis
687 elongation. PLoS biology. 2012;10: e1001415. doi: 10.1371/journal.pbio.1001415.
688 32. Dubrulle J, Pourquie O. fgf8 mRNA decay establishes a gradient that couples axial
689 elongation to patterning in the vertebrate embryo. Nature. 2004;427: 419-422. doi:
690 10.1038/nature02216.
691 33. Muller P, Rogers KW, Yu SR, Brand M, Schier AF. Morphogen transport. Development.
692 2013;104: 1621-1628. doi: 10.1242/dev.083519
693 34. Atsuta Y, Takahashi Y. FGF8 coordinates tissue elongation and cell epithelialization during
694 early kidney tubulogenesis. Development. 2015;142 :2329-2337. doi: 10.1242/dev.122408.

695 35. Olivera-Martinez I, Schurch N, Li RA, Song J, Halley PA, Das RM, et al. Major
696 transcriptome re-organisation and abrupt changes in signaling, cell cycle and chromatin
697 regulation at neural differentiation in vivo. Development. 2014;141: 3266-3276. doi:
698 10.1242/dev.112623.
699 36. Eroshkin FM, Nesterenko AM, Borodulin AV, Martynova NY, Ermakova GV, Gyoeva FK,
700 et al. Noggin4 is a long-range inhibitor of Wnt8 signalling that regulates head development
701 in Xenopus laveis. Sci Rep. 2016;6: 23049. doi: 10.1038/srep23049.
702 37. Niederreither K, McCaffrey P, Dräger UC, Chambon P, Dollé P. Restricted expression and
703 retinoic acid-induced downregulation of the retinaldehyde dehydrogenase type 2 (RALDH-2)
704 gene during mouse development. Mech Dev. 1997;62: 67-78. doi: 10.1016/s0925-
705 4773(96)00653-3.
706 38. White RJ, Nie Q, Lander AD, Schilling TF. Complex regulation of cyp26a1 creates a robust
707 retinoic acid gradient in the zebrafish embryo. PLoS Biology. 2007;5: e304. doi:
708 10.1371/journal.pbio.0050304.
709 39. Gaunt SJ, Drage D, Trubshaw RC. cdx4/lacZ and cdx2/lacZ protein gradients formed by
710 decay during gastrulation in the mouse. Int J Dev Biol. 2005;49:901-908. doi:
711 10.1387/ijdb.052021sg.
712 40. Lunn JS, Fishwick KJ, Halley PA, Storey KG. A spatial and temporal map of FGF/Erk1/2
713 activity and response repertoires in the early chick embryo. Dev Bio. 2007;302:536-552. doi:
714 10.1016/j.ydbio.2006.10.014.
715 41. Vitobello A, Ferretti E, Lampe X, Vilain N, Ducret S, Ori M, et al. Hox and Pbx factors
716 control retinoic acid synthesis during hindbrain segmentation. Dev Cell. 2011;20: 469-482.
717 doi: 10.1016/j.devcel.2011.03.011.

718 42. Kumar S, Duester G. Retinoic acid controls body axis extension by directly repressing Fgf8
719 transcription. Development. 2014;141: 2972-2977. doi: 10.1242/dev.112367.
720 43. Cunningham TJ, Colas A, Duester G. Early molecular events during retinoic acid induced
721 differentiation of neuromesodermal progenitors. Biol Open. 2016;5:1821-1833. doi:
722 10.1242/bio.020891.
723 44. Boulet AM, Capecchi MR. Signaling by FGF4 and FGF8 is required for axial elongation of
724 the mouse embryo. Dev Bio. 2012;371: 235-245. doi: 10.1016/j.ydbio.2012.08.017.
725 45. Bel-Vialar S, Itasaki N, Krumlauf R. Initiating Hox gene expression: in the early chick neural
726 tube differential sensitivity to FGF and RA signaling subdivides the HoxB genes in two
727 distinct groups. Development. 2002;129: 5103-5115.
728 46. Tamashiro DA, Alarcon VB, Marikawa Y. Nkx1-2 is a transcriptional repressor and is
729 essential for the activation of Brachyury in P19 mouse embryonal carcinoma cell.
730 Differentiation. 2012;83: 282-292. doi: 10.1016/j.diff.2012.02.010.
731 47. Takemoto T, Uchikawa M, Kamachi Y, Kondoh H. Convergence of Wnt and FGF signals in
732 the genesis of posterior neural plate through activation of the Sox2 enhancer N-1.
733 Development. 2006;133: 297-306. doi: 10.1242/dev.02196.
734 48. Nordstrom U, Maier E, Jessell TM, Edlund T. An early role for WNT signaling in specifying
735 neural patterns of Cdx and Hox gene expression and motor neuron subtype identity. PLoS
736 Biology. 2006;4: e252. doi: 10.1371/journal.pbio.0040252.
737 49. Novitch BG, Wichterle H, Jessell TM, Sockanathan S. A requirement for retinoic acid-
738 mediated transcriptional activation in ventral neural patterning and motor neuron
739 specification. Neuron. 2003;40: 81-95. doi: 10.1016/j.neuron.2003.08.006

740 50. Sasai N, Kutejova E, Briscoe J. Integration of signals along orthogonal axes of the vertebrate
741 neural tube controls progenitor competence and increases cell diversity. PLoS Biology.
742 2014;12: e1001907. doi: 10.1371/journal.pbio.1001907.
743 51. Pownall ME, Isaacs HV, Slack JM. Two phases of Hox gene regulation during early
744 Xenopus development. Curr Biol. 1998;8: 673-676. doi: 10.1016/s0960-9822(98)70257-x.
745 52. Oates AC, Morelli LG, Ares S. Patterning embryos with oscillations: structure, function and
746 dynamics of the vertebrate segmentation clock. Development. 2012;139:625-639. doi:
747 10.1242/dev.063735.
748 53. Isaacs HV, Pownall ME, Slack JM. Regulation of Hox gene expression and posterior
749 development by the Xenopus caudal homologue Xcad3. EMBO J. 1998;17: 3413-3427. doi:
750 10.1093/emboj/17.12.3413.
751 54. Amin S, Neijts R, Simmini S, van Rooijen C, Tan SC, Kester L, et al. Cdx and T Brachyury
752 Co-activate Growth Signaling in the Embryonic Axial Progenitor Niche. Cell Rep. 2016;17:
753 3165-3177. doi: 10.1016/j.celrep.2016.11.069.
754 55. Castillo HA, Cravo RM, Azambuja AP, Simoes-Costa MS, Sura-Trueba S, Gonzalez J, et al.
755 Insights into the organization of dorsal spinal cord pathways from an evolutionarily
756 conserved raldh2 intronic enhancer. Development. 2010;137: 507-518. doi:
757 10.1242/dev.043257.

758

759 # SUPPLEMENTARY INFORMATION

760 ## Supplementary methods

761 1. General Hill functions

762 2. In situ hybridization

763

764 # Supplementary figures

765 **Fig S1. Hill constant determine the strength of response of targets to activators and**
766 **repressors.** Temporal response of targets with different Hill constants to activators and
767 repressors. Inputs are shown in blue and targets with different Hill constants are color coded:
768 H1=1, orange; H2=10, yellow; H3=20, purple; and H4=100, green. **(A-B)** For activators,
769 constant (A) and graded (B) inputs induce targets with smaller Hill constants to higher levels
770 than targets with larger Hill constants. (**C-D**) For repressors, constant (C) and graded (D) inputs
771 reduce targets with smaller Hill constants to lower levels than targets with larger Hill constants.
772 With graded inputs (B, D), larger Hill constants also cause temporal delays in response.

773

774 **Fig S2. Changes in FGF-WNT-RA signaling interactions results in mRNA profiles parallel**
775 **protein accumulation and are stable over time.** (**A**) Profiles of mRNA transcripts at t=6000
776 min associated with production of signaling molecules. Transcript and protein profiles are
777 similar (**Fig 2C** left panels). (**B**) Signaling molecule profiles are stable over longer simulation
778 times. An FGF-RA balance simulation that was run for t=30,000 min produced the same profile
779 than a simulation that was run for t=6000 min (**Fig 2C** middle row).

780

781 **Fig S3. RA positive autoregulation is required for bistability.** Reducing RA's positive effect
782 on *Raldh2* transcription (H= 300 instead of 50) results in aberrant RA, but not FGF, distribution.
783 (**A**) Under these conditions, when FGF affinity to repress *Raldh2* is strong (H=2 instead of 10), a
784 peak of RA production forms at a position in the field where the FGF-RA switch would have

occurred (1500-2000 μm). (**B**) When RA repression of *Fgf8* transcription is weakened (H=20 instead of 1), RA production oscillates in the region of cell differentiation (>1500 μm).

Fig S4. Stability of the transcription profile in the parameter space. Changes in the strength of interactions between transcriptional factors does not drastically affect the transcriptional domain profile. (**A**) Original transcription profile as shown in Fig 4F. (**B, C**) Reducing (B) or increasing (C) all the Hill constants in the interaction network by 30% does not significantly change the spatial profile of gene transcription.

APPENDIX

SIGNET.m: MATLAB code for simulating signaling dynamics.

TRANSNET.m: MATLAB code for simulating transcriptional factor dynamics.

SUPPLEMENTAL INFORMATION

Supplementary methods

Hill functions describing general regulatory interactions

The Hill functions H_1, H_2, H_3, H_4 were used in the transcription and translation equations to describe one of four different types of interactions: (1) inductive, (2) repressive, (3) coordinated and (4) competitive. We generated transcription and translation equations specific for each factor by replacing H_1, H_2, H_3, and H_4 with the functions that represent the regulatory interactions reported experimentally.

INDUCTIVE INTERACTIONS. H_i, describes the input of one or multiple activators and can take three different forms.

H_i for a single activator is of the form:

$$H_i = \frac{\left(\frac{A}{A_c}\right)^n}{1 + \left(\frac{A}{A_c}\right)^n}$$

H_i for two activators, when both activators are necessary to stimulate activity (Boolean AND), is of the form:

$$H_i = \frac{\left(\frac{A1}{A1_c}\right)^{n1}}{1 + \left(\frac{A1}{A1_c}\right)^{n1}} \, x \, \frac{\left(\frac{A2}{A2_c}\right)^{n2}}{1 + \left(\frac{A2}{A2_c}\right)^{n2}}$$

H_i for two activators, when one activator is sufficient to stimulate activity (Boolean OR), is of the form:

$$H_i = \frac{\left(\frac{A1}{A1_c}\right)^{n1} + \left(\frac{A2}{A2_c}\right)^{n2}}{1 + \left(\frac{A1}{A1_c}\right)^{n1} + \left(\frac{A2}{A2_c}\right)^{n2}}$$

, where, for all these equations, $A, A1, A2$ are the concentrations of activator proteins; $A_c, A1_c, A2_c$ are the respective Hill constants; and *n, n1, n2* are the Hill coefficient of cooperativity.

REPRESSIVE INTERACTIONS. H_i, describes the input of one or multiple repressors and can take three different forms.

H_i for a single repressor is of the form:

$$H_i = \frac{1}{1 + \left(\frac{R}{R_c}\right)^m}$$

H_i for two repressors, when both repressors are necessary for downregulation (Boolean AND), is of the form:

$$H_i = \frac{1}{1 + \left(\frac{R1}{R1_c}\right)^{m1}} x \frac{1}{1 + \left(\frac{R2}{R2_c}\right)^{m2}}$$

H_i for two repressors, when one repressor is sufficient for downregulation (Boolean OR), is of the form:

$$H_i = \frac{1}{1 + \left(\frac{R1}{R1_c}\right)^{m1} + \left(\frac{R2}{R2_c}\right)^{m2}}$$

, where, for these equations, $R, R1, R2$ are the concentration of repressor proteins; $R_c, R1_c, R2_c$ are the respective Hill constants; and *m, m1, m2* are the Hill coefficients of cooperativity.

COORDINATED INTERACTIONS. H_i, describes the input of multiple activators and repressors working simultaneously through separate regulatory sites.

$$H_i = \frac{\left(\frac{A}{A_c}\right)^n}{1 + \left(\frac{A}{A_c}\right)^n} x \frac{1}{1 + \left(\frac{R}{R_c}\right)^m}$$

, where, for these equations, A, R are the concentration of activator and repressor proteins; A_c, R_c are the respective Hill constants; and *m, n* are the Hill coefficients of cooperativity.

COMPETITIVE INTERACTIONS. H_i, describes the input of multiple activators and repressors working simultaneously through the same regulatory sites.

$$H_i = \frac{\left(\frac{A}{A_c}\right)^n}{1 + \left(\frac{A}{A_c}\right)^n + \left(\frac{R}{R_c}\right)^m}$$

, where, for these equations, A, R are the concentration of activator and repressor proteins; A_c, R_c are the respective Hill constants; and *m, n* are the Hill coefficients of cooperativity.

Hill constants measure the interaction strength between the activators/repressors and their target gene, and are defined as the concentration of the regulator at which the rate of gene activation or repression is half the synthesis rate maximum [1]. The hypothetical range for Hill constants is from zero to infinity, with low Hill values signify strong and fast regulatory activities while high Hill values signifying weak and slow regulatory activities (**Fig S1**).

In situ hybridization

Analysis of gene transcription by *in situ* hybridization was done using digoxigenin (DIG)-labeled antisense RNA probes synthesized and hybridized using standard protocol [2], as previously described [3]. Briefly, embryos were harvested at the appropriate stage and fixed with 4% paraformaldehyde diluted in 1x PBS at 4° C overnight. After a series of washes, embryos were exposed overnight in hybridization solution to DIG-labeled antisense RNA probes against *Pax6*, *Nkx1.2*, *Bra*, *Sox2*, *Cdx4 or Ngn2*. mRNA expression was detected using an Alkaline Phosphatase coupled Anti-DIG antibody (Roche) and developing embryos with nitro-blue

58 tetrazolium salt (NBT, Thermo Scientific) and 5-bromo-4-chloro-3-indolyl-phosphate (BCIP,
59 Biosynth) at room temperature until dark purple precipitate deposited revealing the areas of gene
60 transcription. Post-development, embryos were washed with 1x TBST and then fixed in 4%
61 PFA. Processed embryos were photographed using an AxioCam MRc digital color camera
62 mounted on a Zeiss V20 Stereo microscope and processed using Adobe Photoshop (CC2017,
63 Adobe) for size and resolution adjustment and figure preparation.

64

65 References (Supplemental Methods)

66 1. Santillan M. On the Use of the Hill Functions in Mathematical Models of Gene Regulatory
67 Networks. Math Mod Nat Phenom. 2008;3:85-97. doi: 10.1051/mmnp:2008056.
68 2. Wilkinson DG, Nieto MA. Detection of messenger RNA by in situ hybridization to tissue sections
69 and whole mounts. Meth Enzymol. 1993;225: 361-373. DOI: 10.1016/0076-6879(93)25025-w
70 3. Joshi P, Darr AJ, Skromne I. CDX4 regulates the progression of neural maturation in the spinal
71 cord. Dev Bio. 2019. doi: 10.1016/j.ydbio.2019.02.014.

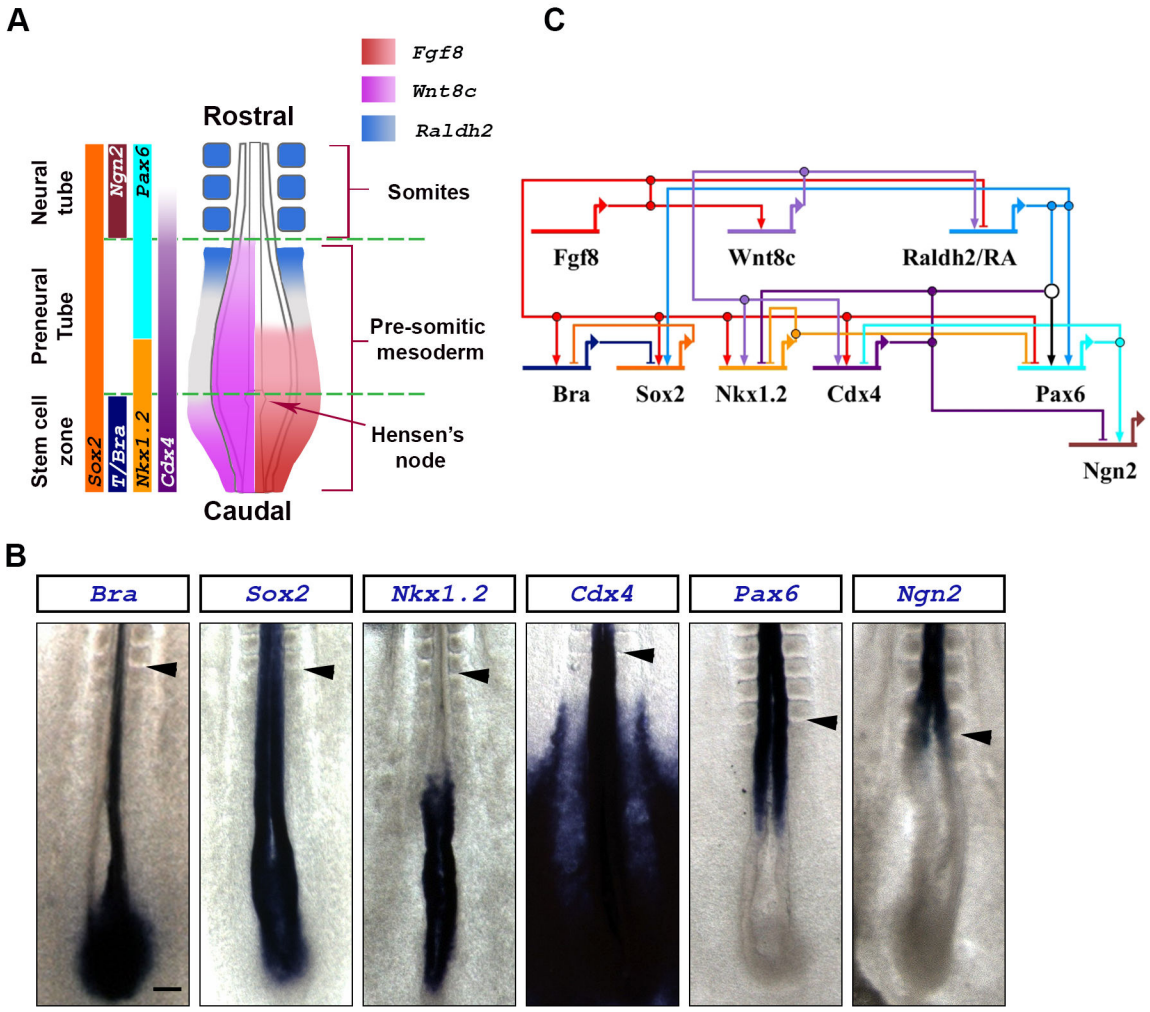
A
Fgf8
Wnt8c
Raldh2
Rostral
Caudal
Neural tube
Preneural Tube
Stem cell zone
Ngn2
Pax6
Sox2
T/Bra
Nkx1.2
Cdx4
Somites
Pre-somitic mesoderm
Hensen's node
C
Fgf8
Wnt8c
Raldh2/RA
Bra
Sox2
Nkx1.2
Cdx4
Pax6
Ngn2
B
Bra
Sox2
Nkx1.2
Cdx4
Pax6
Ngn2

Figure 1

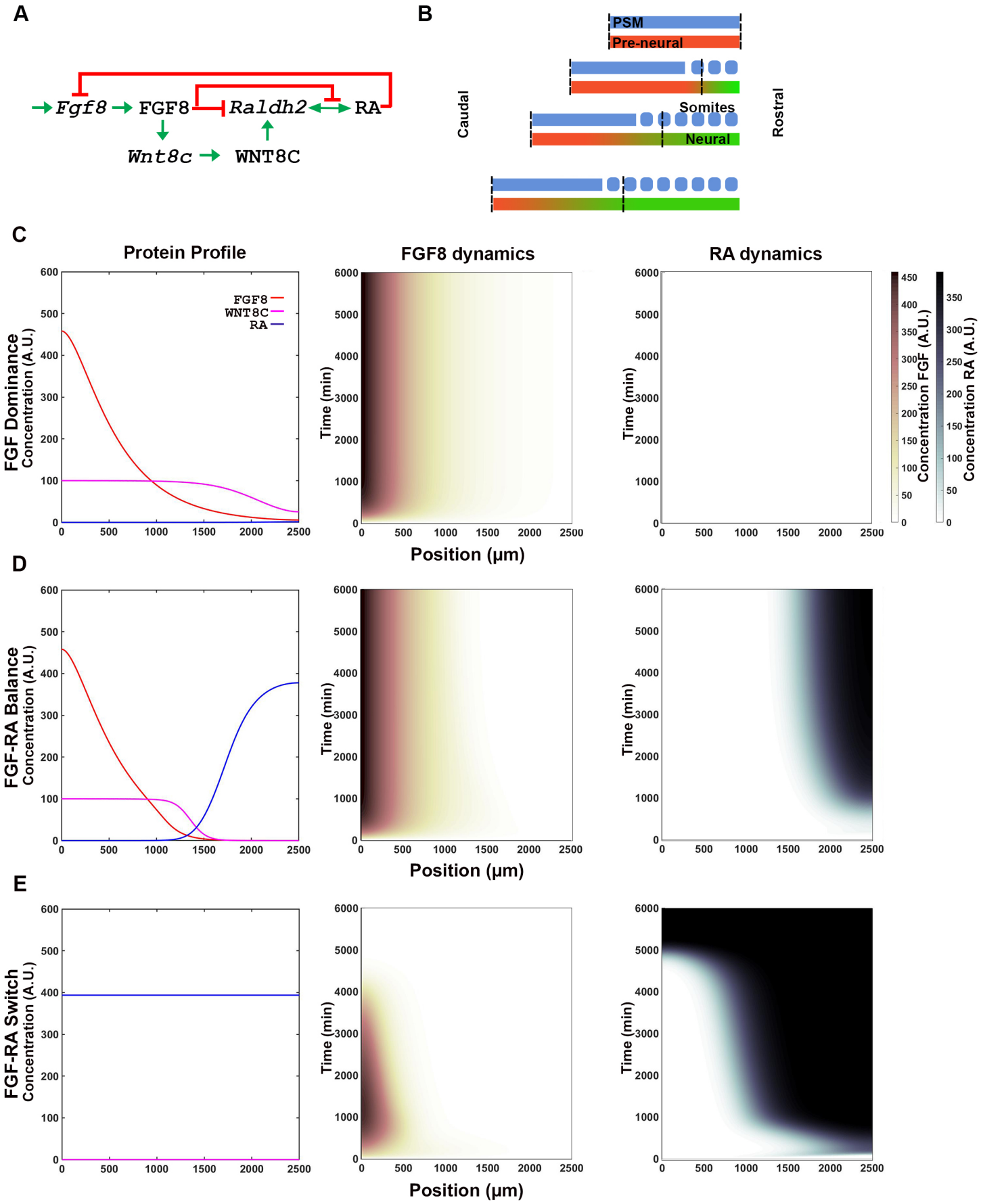
A
Fgf8
FGF8
Raldh2
RA
Wnt8c
WNT8C
B
PSM
Pre-neural
Caudal
Rostral
Somites
Neural
C
Protein Profile
FGF8 dynamics
RA dynamics
FGF8
WNT8C
RA
FGF Dominance
Concentration (A.U.)
Time (min)
Position (μm)
Concentration FGF (A.U.)
Concentration RA (A.U.)
D
FGF-RA Balance
E
FGF-RA Switch

Figure 2

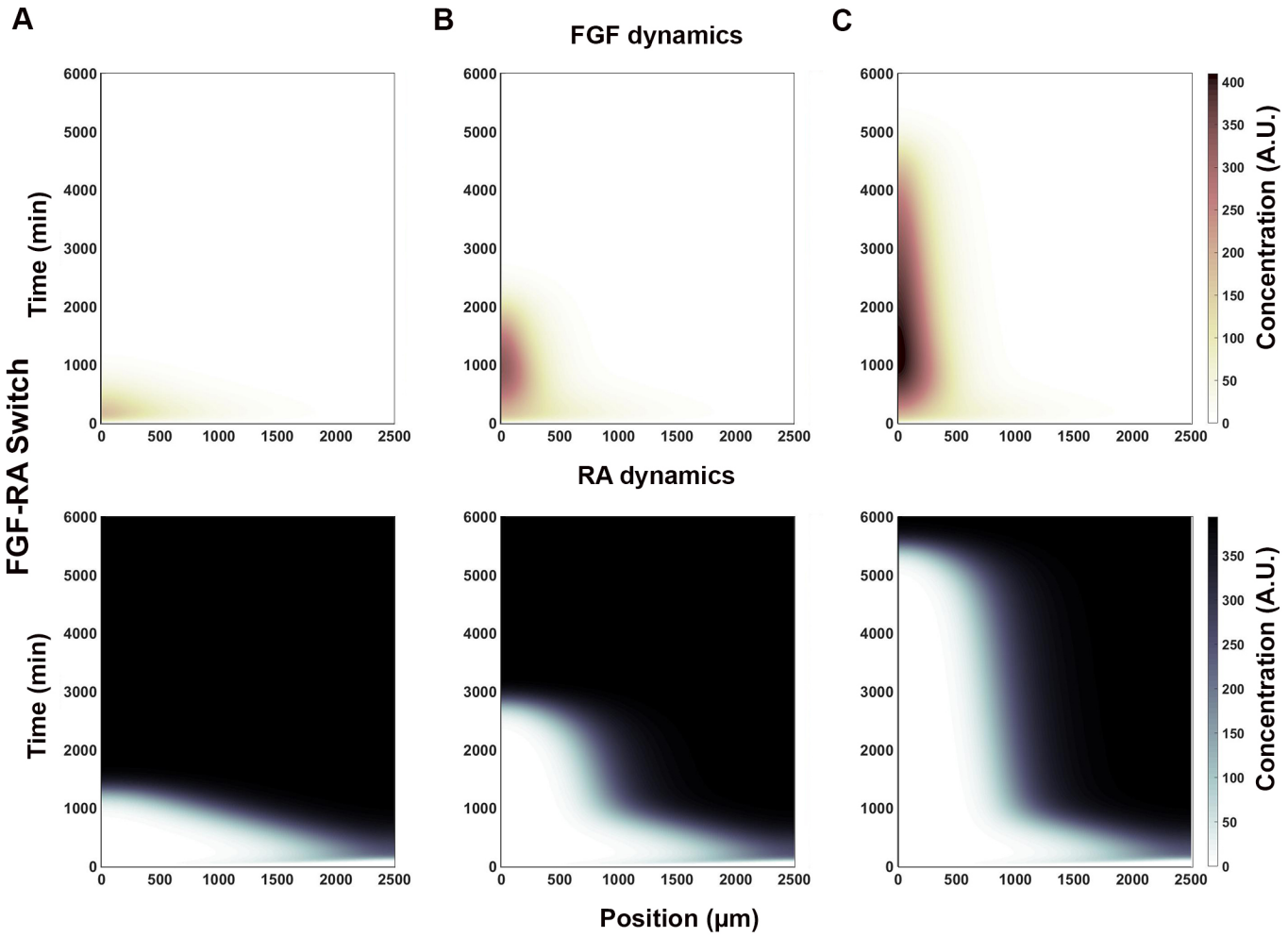
A
B
C
FGF dynamics
RA dynamics
FGF-RA Switch
Time (min)
Position (μm)
Concentration (A.U.)
0
1000
2000
3000
4000
5000
6000
500
1500
2500
50
100
150
200
250
300
350
400

Figure 3

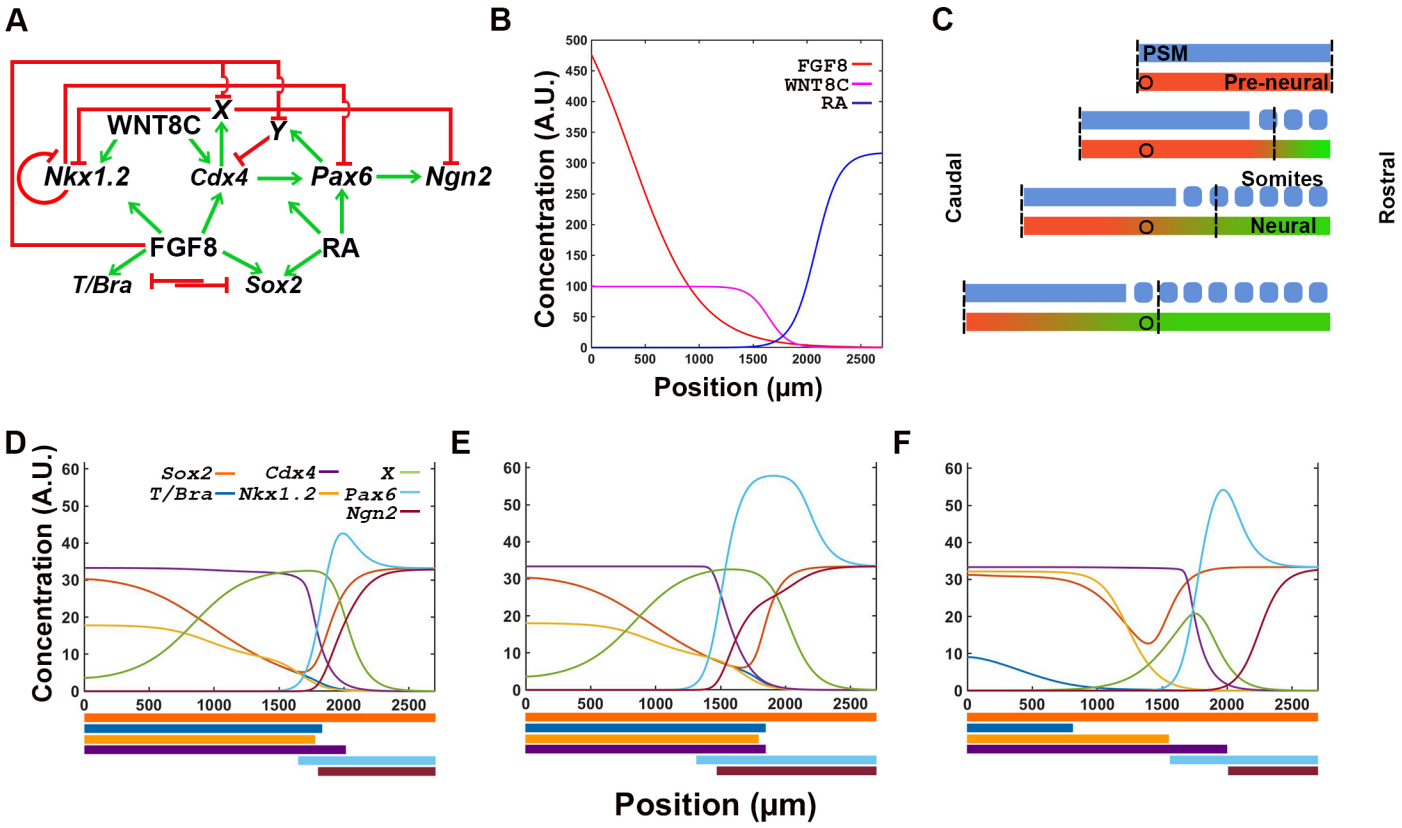
A
WNT8C
X
Y
Nkx1.2
Cdx4
Pax6
Ngn2
FGF8
RA
T/Bra
Sox2
B
FGF8
WNT8C
RA
Concentration (A.U.)
Position (μm)
C
PSM
Pre-neural
Somites
Neural
Caudal
Rostral
D
E
F
Sox2
Cdx4
X
T/Bra
Nkx1.2
Pax6
Ngn2
Concentration (A.U.)
Position (μm)

Figure 4

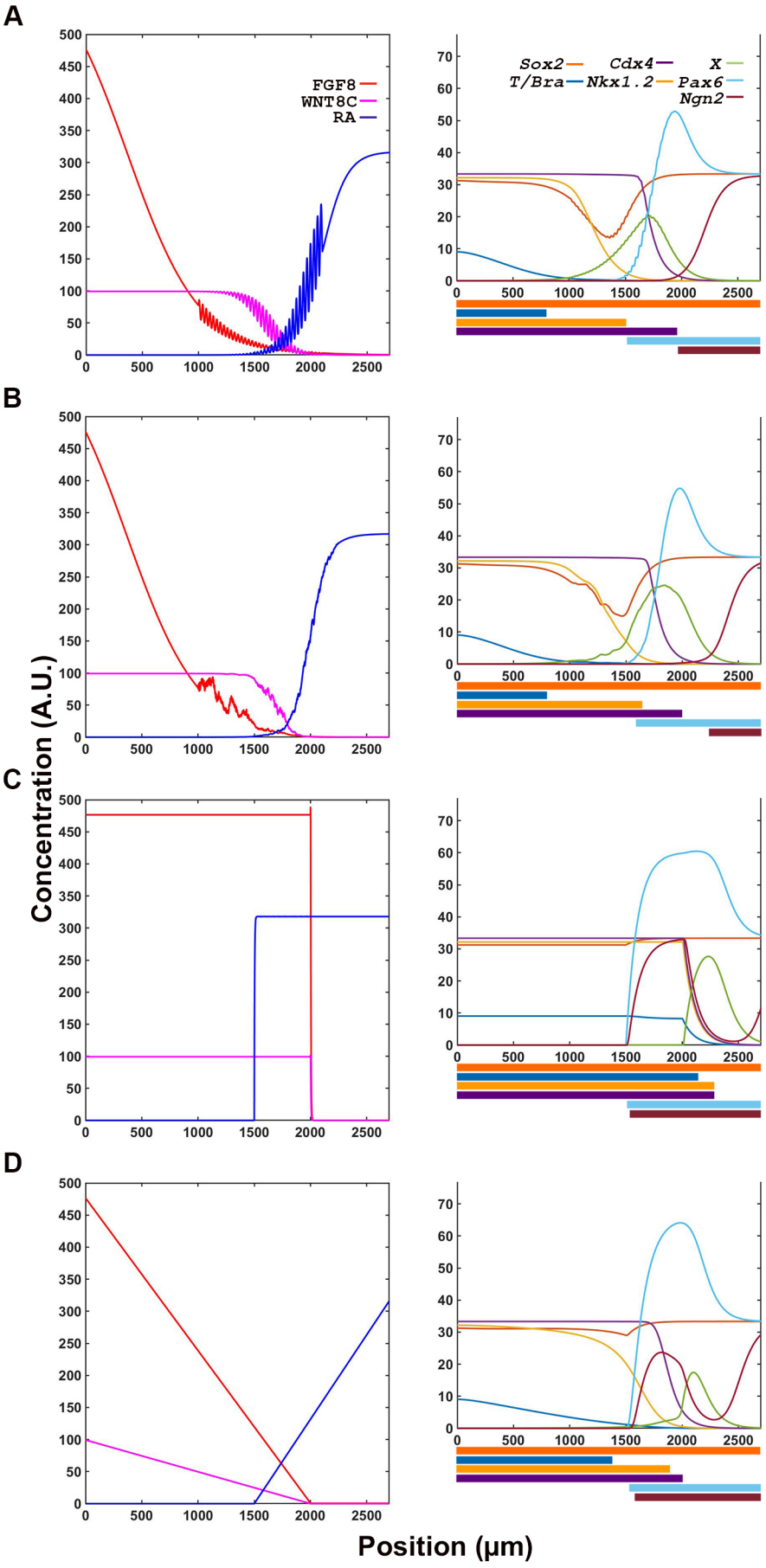
A
B
C
D
FGF8
WNT8C
RA
Sox2
Cdx4
X
T/Bra
Nkx1.2
Pax6
Ngn2
Concentration (A.U.)
Position (μm)

Figure 5

Figure 6

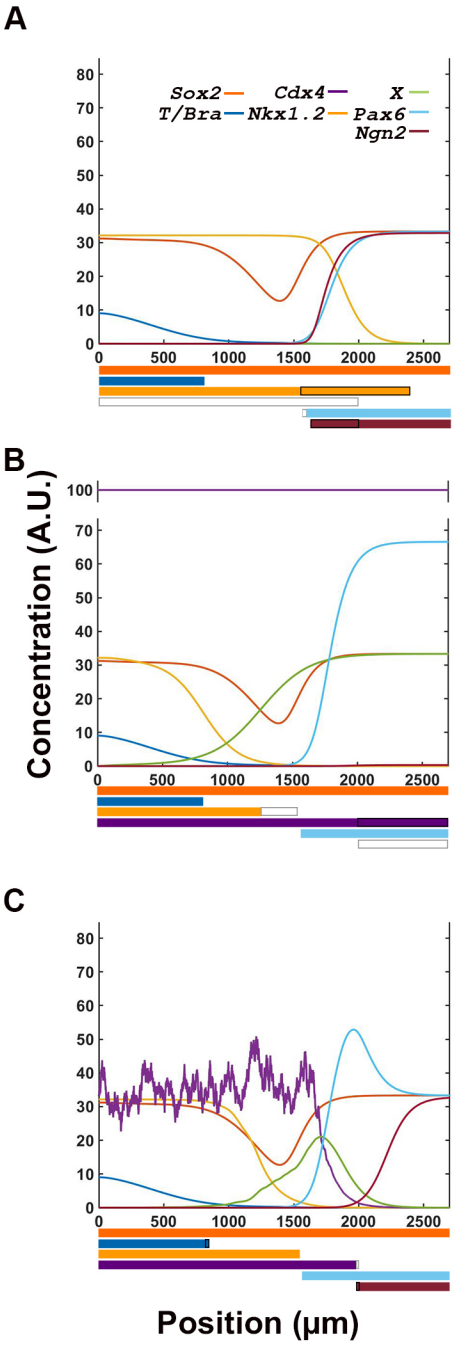
A
Sox2
Cdx4
X
T/Bra
Nkx1.2
Pax6
Ngn2
B
C
Concentration (A.U.)
Position (μm)

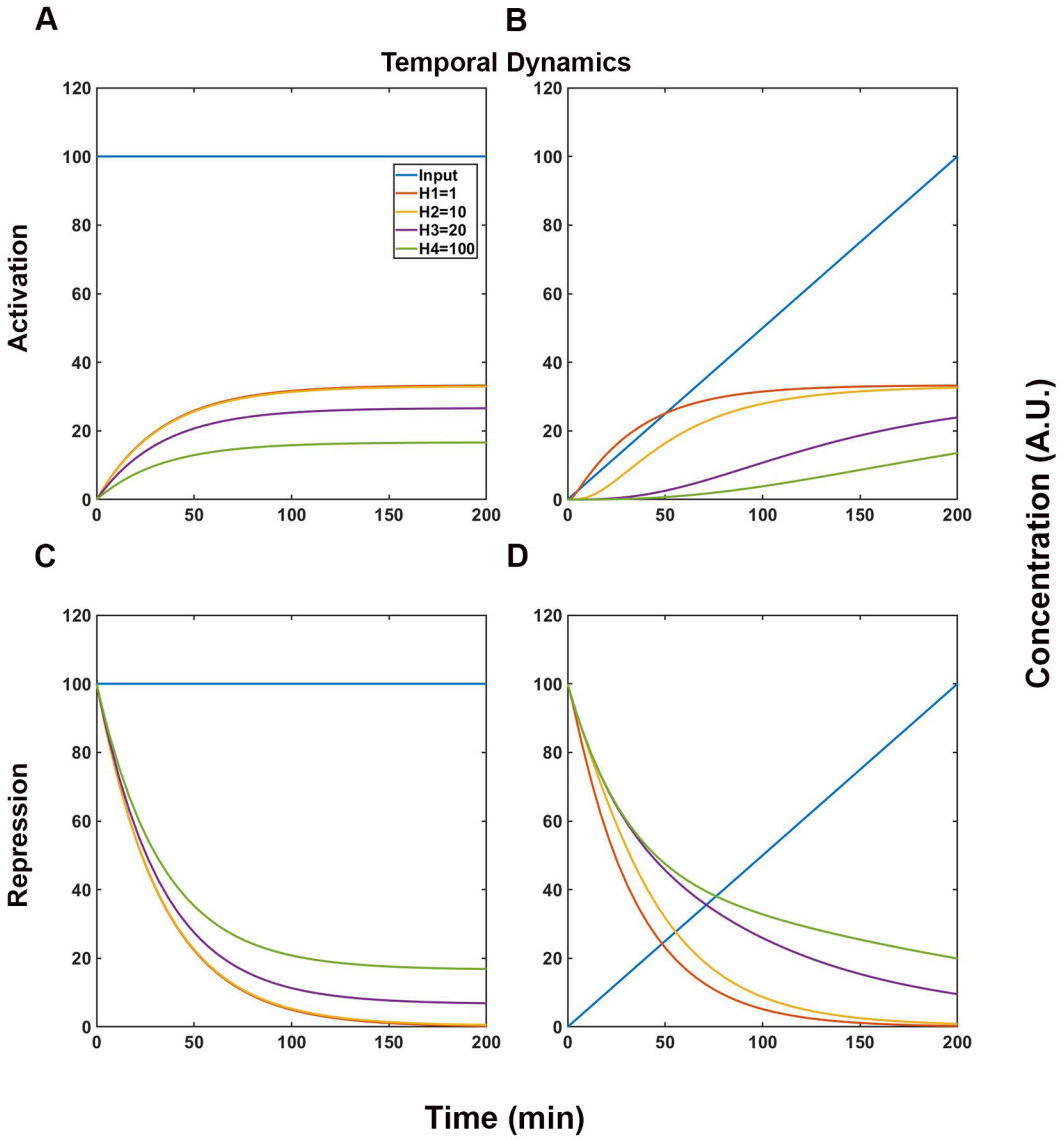
A
B
Temporal Dynamics
Activation
Input
H1=1
H2=10
H3=20
H4=100
C
D
Repression
Concentration (A.U.)
Time (min)

Figure S1

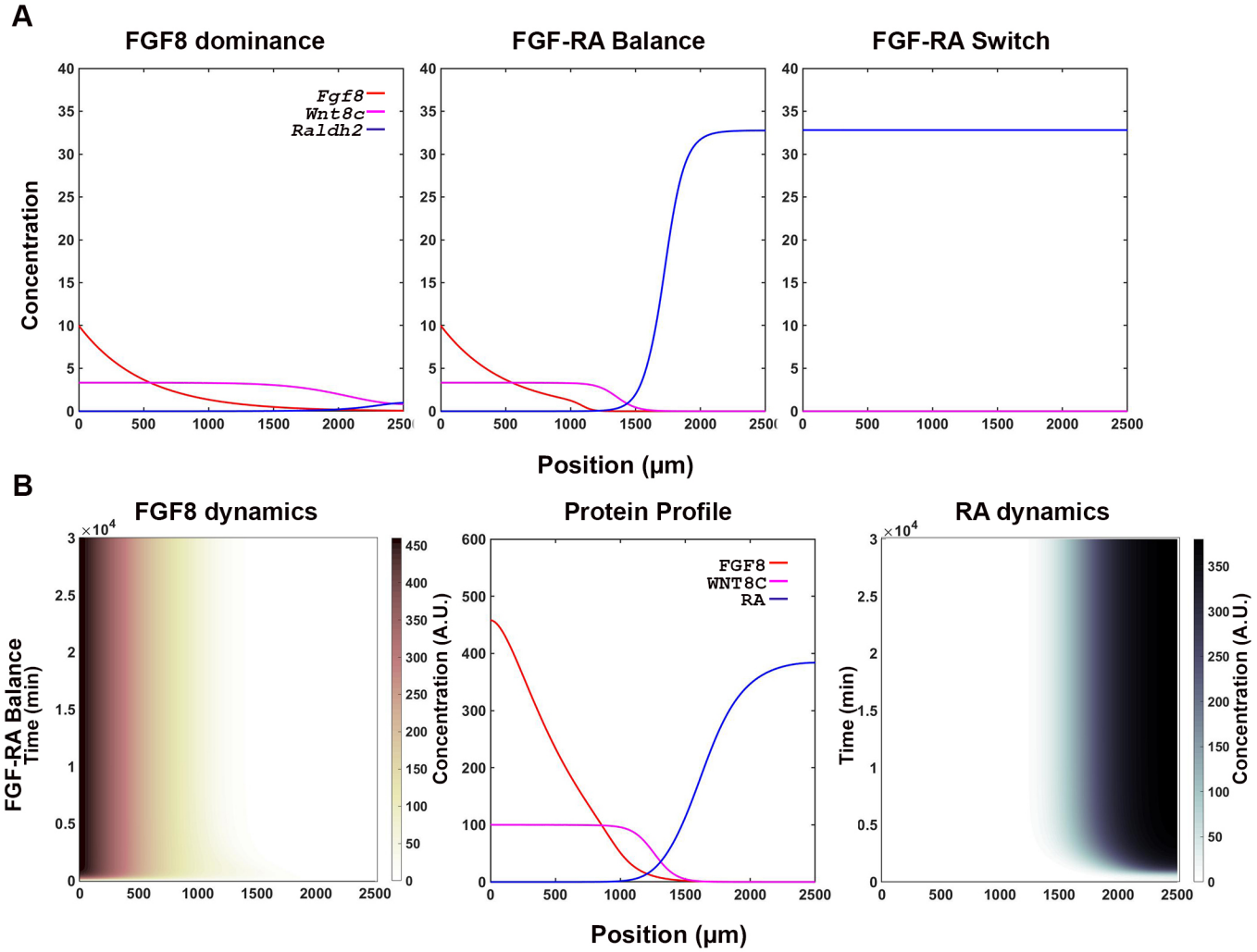
A
FGF8 dominance
FGF-RA Balance
FGF-RA Switch
Fgf8
Wnt8c
Raldh2
Concentration
Position (μm)
B
FGF8 dynamics
Protein Profile
RA dynamics
FGF-RA Balance
Time (min)
Concentration (A.U.)
FGF8
WNT8C
RA
Time (min)
Concentration (A.U.)
Position (μm)

Figure S2

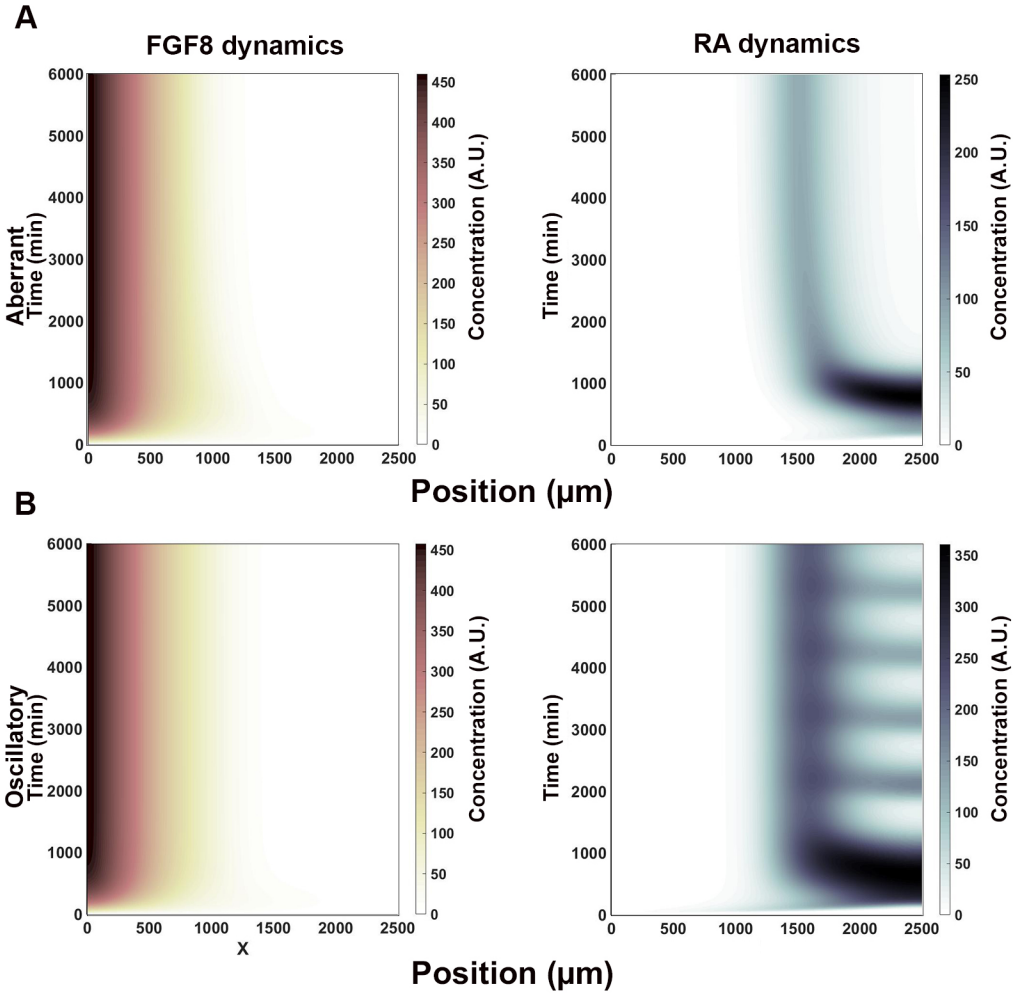
A
FGF8 dynamics
RA dynamics
Aberrant
Time (min)
Concentration (A.U.)
Position (μm)
B
Oscillatory
Time (min)
Concentration (A.U.)
x
Position (μm)

Figure S3

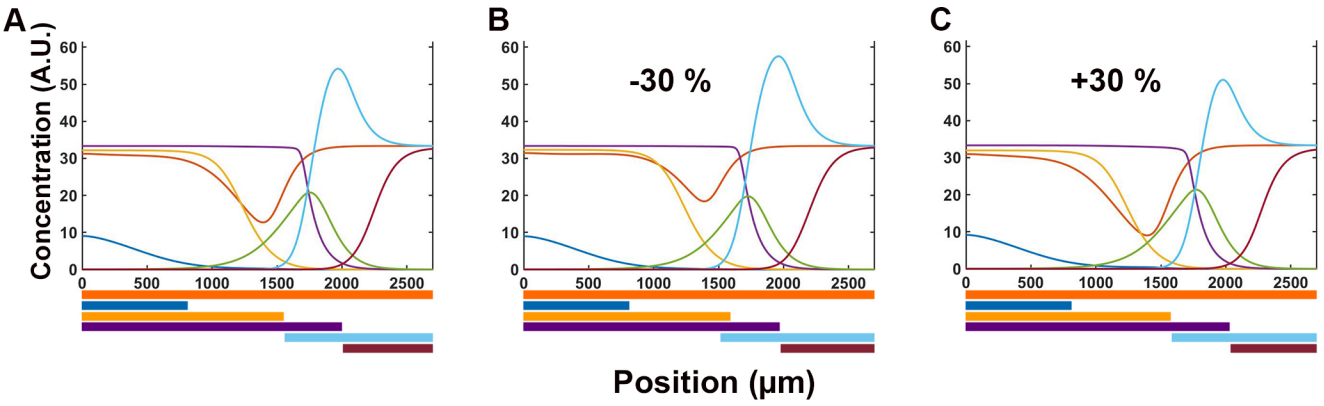
A
B
C
-30 %
+30 %
Concentration (A.U.)
Position (μm)
0
10
20
30
40
50
60
500
1000
1500
2000
2500

Figure S4